이학석사 학위논문

# Effect of Temperature and Iron Content on Structure and Disorder in Oxide: Insights from High-Resolution Solid-State NMR Study of Aluminum (oxy)Hydroxide Polymorphs and Iron-bearing Silicate Glasses

# 고분해능 고상 핵자기공명 분광분석을 이용한 수산화알루미늄 동질이상의 상전이 기작과 철의 함량에 따른 비정질 Fe-규산염의 원자구조 및 무질서도 변화에 대한 원자단위의 고찰

2011 년 8 월

서울대학교 대학원
자연과학대학 지구환경과학부
김 효 임

# Effect of Temperature and Iron Content on Structure and Disorder in Oxide: Insights from High-Resolution Solid-State NMR Study of Aluminum (oxy)Hydroxide Polymorphs and Iron-bearing Silicate Glasses

# 고분해능 고상 핵자기공명 분광분석을 이용한 수산화알루미늄 동질이상의 상전이 기작과 철의 함량에 따른 비정질 **Fe-**규산염의 원자구조 및 무질서도 변화에 대한 원자단위의 고찰

지도교수: 이성근

이 논문을 이학석사 학위논문으로 제출함

2011년 8월


서울대학교 대학원

자연과학대학 지구환경과학부

김효임


김효임의 이학석사 학위논문을 인준함

2011년 8월

| | | |
|---|---|---|
| 위 원 장 | 조 문 섭 | (인) |
| 부위원장 | 이 성 근 | (인) |
| 위 원 | 허 영 숙 | (인) |

**Abstract**

Diverse geological processes in the Earth's surfaces and interiors are controlled by the macroscopic thermodynamics and transport properties of crystalline and non-crystalline Earth materials. These properties depend on their atomic structure with varying temperature and composition. However, the detailed temperature-induced structural changes in aluminum (oxy)hydroxide polymorphs at low temperature and structure and disorder in iron-bearing silicate glasses and melts at high temperature are not fully understood. In this study, we explore the detailed temperature-induced structural changes in aluminum (oxy)hydroxide polymorphs up to 300°C using high-resolution $^{27}$Al MAS NMR. We also attempt to unveil the effect of iron content on the structure (the degree of network polymerization) and the extent of disorder in iron-bearing sodium silicate glasses using Raman spectroscopy and multi-nuclear NMR.

Structural transitions involving metastable phases at low temperature, such as aluminum (oxy)hydroxide polymorphs allow us to provide better understanding of natural processes in Earth's surfaces such as diagenesis and weathering. We first investigate the temperature-induced structural changes in aluminum (oxy)hydroxide polymorphs (boehmite, gibbsite, and bayerite) and their phase transition to metastable alumina using high-resolution NMR. The $^{27}$Al MAS NMR spectra show previously unknown detailed changes in Al coordination environment upon transition into γ-$Al_2O_3$ and η-$Al_2O_3$: the fraction of $^{[4]}$Al and peak widths of $^{[6]}$Al in aluminum (oxy)hydroxide polymorphs increase with increasing

temperature. The detailed structural transition, however, shows distinct transition behaviors. Upon transition from boehmite to γ-$Al_2O_3$, the fraction of $^{[4,5]}$Al increase gradually with increasing temperature up to 300°C. Transition from gibbsite to γ-$Al_2O_3$, however, were characterized with an abrupt increase in $^{[4]}$Al fraction with temperature. The transition from bayerite to η-$Al_2O_3$ exhibits similar trend where abrupt coordination transformation within a narrow temperature range is observed. The presence of $^{[5]}$Al in boehmite and its absence in other polymorphs suggest a larger topological disorder in the former and may be responsible for the observed gradual coordination transformation. These results suggest that the detailed of structural transition in aluminum (oxy)hydroxide depends both on the types of precursors and temperature. The current results with prototypical single-component of aluminum (oxy)hydroxide can provide atomistic link to the structural phase transition in complex and multi-component oxide in the Earth's surfaces.

The presence of iron in Earth materials affects their atomic structures and has significant geochemical implications for diverse igneous processes involving mid-ocean ridge magmatism and seismic heterogeneity at the core-mantle boundary. Despite these geochemical and geophysical implications, revealing the atomic structure and disorder in iron-bearing silicate melts and glasses remains a fundamental yet difficult problem in geochemistry, glass sciences, and physical chemistry due to lack of suitable experimental structural probe of iron-bearing silicate glasses. Here, we report experimental results on the effect of iron content on the structure and disorder in iron-bearing sodium silicate glasses (up to 34.60 wt% $Fe_2O_3$)

using Raman and $^{29}Si$ and $^{17}O$ solid-state NMR [1D MAS and 2D triple quantum (3Q) MAS] spectroscopy. Raman spectra for iron-bearing sodium silicate glasses with varying iron content probe the potential variation in $Q^n$ (where n refers to the number of bridging oxygen per tetrahedrally coordinated cation) species with increasing iron content. $^{29}Si$ $T_1$ relaxation time for the glasses decreases with increasing iron content due to an enhanced interaction between nuclear spin and unpaired electron in Fe. $^{29}Si$ and $^{17}O$ MAS NMR spectra for the glasses with varying iron content also show a decrease in signal intensity and an increase in peak width with increasing iron content. However, the heterogeneous peak broadening in both $^{29}Si$ and $^{17}O$ MAS NMR spectra suggests the heterogeneous distribution of $Q^n$ species and oxygen clusters around iron in iron-bearing silicate glasses. $^{17}O$ MAS NMR spectra for the glasses show well-resolved non-bridging oxygen (NBO, Na-O-Si) and bridging oxygen (BO, Si-O-Si) sites even at relatively high iron concentration (~34.60 wt% $Fe_2O_3$). The fraction of NBO apparently decreases with iron content, implying that iron can play a dual role as both network modifying and network forming cations. The peak widths of NBO and BO in isotropic dimension increase with iron content. The result indicates that life-time broadening due to spin-electron interaction is significantly larger than quadrupolar interaction. These results demonstrate that solid-state NMR, particularly $^{17}O$ 3QMAS NMR can be an effective probe of the detailed structure and the extent of disorder in iron-bearing silicate glasses. It may also provide an atomistic explanation for effect of iron content on the element partitioning between crystals and melts, entropy, and viscosity of iron-bearing silicate melts and

glasses.

## Tables of Contents

## List of Figures

**Figure 9.** Normalized Raman spectra for iron-bearing sodium silicate glasses at 9.4 T with varying $X_{Fe_2O_3}$ [=$Fe_2O_3$/($Fe_2O_3$+$Na_2O$)], as labeled.

**Figure 10.** $^{29}$Si MAS NMR spectra for iron-bearing sodium silicate glasses at τ from 0.0003 to 0.1 s with varying $X_{Fe_2O_3}$ [=$Fe_2O_3$/($Fe_2O_3$+$Na_2O$)], as labeled.

**Figure 11.** $\log_{10}$-$\log_{10}$ plot of $^{29}$Si $T_1$ relaxation (saturation-recovery) data for iron-bearing sodium silicate glasses at 9.4 T with varying $X_{Fe_2O_3}$ [=$Fe_2O_3$/($Fe_2O_3$+$Na_2O$)], as labeled.

**Figure 12.** $^{29}$Si MAS NMR for iron-bearing sodium silicate glasses at 9.4 T with varying $X_{Fe_2O_3}$ [=$Fe_2O_3$/($Fe_2O_3$+$Na_2O$)], as labeled. Vertical scale is arbitral unit (not normalized) due to comparison of signal intensity with increasing $X_{Fe_2O_3}$.

**Figure 13.** $^{17}$O MAS NMR spectra for iron-bearing sodium silicate glasses at 9.4 T with varying $X_{Fe_2O_3}$ [=$Fe_2O_3$/($Fe_2O_3$+$Na_2O$)], as labeled. Vertical scale is arbitral unit (not normalized) due to comparison of signal intensity with increasing $X_{Fe_2O_3}$

**Figure 14.** Variation of maximum peak intensity for $^{29}$Si (closed triangle) and $^{17}$O (open circle) MAS NMR spectra with varying $X_{Fe_2O_3}$.

**Figure 15.** $^{29}$Si MAS NMR spectra for iron-bearing sodium silicate glasses at 9.4 T with varying $X_{Fe_2O_3}$ [=$Fe_2O_3$/($Fe_2O_3$+$Na_2O$)], as labeled. The spinning side band is also presented in this Figure. Vertical scale is arbitral unit (not normalized) due to comparison of signal intensity with increasing $X_{Fe_2O_3}$.

**Figure 16.** $^{17}$O MAS NMR spectra for iron-bearing sodium silicate glasses at

9.4 T with varying $X_{Fe_2O_3}$ [=$Fe_2O_3$/($Fe_2O_3$+$Na_2O$)], as labeled. The spinning side band is also presented in this Figure. Vertical scale is arbitral unit (not normalized) due to comparison of signal intensity with increasing $X_{Fe_2O_3}$.

**Figure 17.** Normalized $^{29}$Si MAS NMR spectra for iron-bearing sodium silicate glasses at 9.4 T with varying $X_{Fe_2O_3}$ [=$Fe_2O_3$/($Fe_2O_3$+$Na_2O$)], as labeled.

**Figure 18.** Variation of full width at half maximum (FWHM) of $^{29}$Si MAS NMR spectra for iron-bearing sodium silicate glasses at 9.4 T with varying $X_{Fe_2O_3}$ [=$Fe_2O_3$/($Fe_2O_3$+$Na_2O$)], as labeled.

**Figure 19.** Normalized $^{17}$O MAS NMR spectra for iron-bearing sodium silicate glasses at 9.4 T with varying $X_{Fe_2O_3}$ [=$Fe_2O_3$/($Fe_2O_3$+$Na_2O$)], as labeled.

**Figure 20.** $^{17}$O 3QMAS NMR for iron-bearing sodium silicate glasses at 9.4 T with varying $X_{Fe_2O_3}$ [=$Fe_2O_3$/($Fe_2O_3$+$Na_2O$)], as labeled. Contour lines are drawn from 8% to 98% of relative intensity with a 5% increment and an added line at 6%.

**Figure 21.** Total isotropic projection of $^{17}$O 3QMAS NMR for iron-bearing sodium silicate glasses at 9.4 T with varying $X_{Fe_2O_3}$ [=$Fe_2O_3$/($Fe_2O_3$+$Na_2O$)], as labeled.

## List of Tables

# 1. Introduction

Diverse geological processes in the Earth's surface and interior depend on the macroscopic properties of Earth materials which are determined by their microscopic scale local structure. For example, coordination environment and topological disorder of atoms in silicate melts and glasses play a crucial role in the generation, migration, and dynamics of magma (Lee, 2005; Lee et al., 2010b). Therefore, probing microscopic scale of atomic configuration is essential in understanding and predicting macroscopic properties and diverse geological processes.

Whereas there have been extensive theoretical and experimental studies of the atomic structures of Earth's material, several questions to even very simple and ubiquitous system in nature have remained to unsolved problem. The thermodynamic properties change on atomic structure of metastable/disordered crystal phase (Bokhimi et al., 2001; Hemingway, 1991; Hemingway et al., 1991; Violante and Huang, 1993) and the structural change of silicate melts with increasing iron content are examples of unsolved question. In Earth system, phase transition of metastable or disordered crystal phase in low temperature can considerably affect the surface process such as weathering, diagenesis, dehydration and mixed-layer silicate transition (Pollastro and Bohor, 1993; Sass et al., 1987; Whitney and Northrop, 1988). And effect of iron content on structure in silicate melt can used to infer details about the origin of magma, and also affect physical and chemical properties such as melt structure, viscosity, the behavior of volatile components (Mysen, 2006; Mysen and

Virgo, 1985; Rossano et al., 2000).

Recent advanced in spectroscopic techniques especially for solid-state NMR with developments of experimental techniques yields information that is element specific and allows the determination of short-range structures around elements of interest in diverse amorphous and disorder silicate. Solid-state NMR also has been traditionally effective in carrying out quantitative investigation of atomic structures in amorphous oxide including silicates (Lee et al., 2010b). Development and recent progress in the multiple quantum magic angle spinning (MQMAS, or triple quantum MAS, 3QMAS) experiments provide considerably improved resolution over 1D MAS NMR and have thus proved to be extremely beneficial for resolving the atomic configurations surrounding quadrupolar nuclides. On the basis of these recent studies, detailed information concerning distribution of cations and anions in complex crystalline and non-crystalline solids has begun to be unveiled.

The organization of this thesis is as follows. First, summary of the principles of solid-state NMR spectroscopy used in this study is presented in chapter 2. In this chapter, NMR methodologies which are used to obtain high-resolution signal are also presented. Second, we report high-resolution $^{27}$Al MAS NMR spectra for aluminum (oxy)hydroxide polymorphs with varying annealing temperature to explore the temperature -induced structural change below 300°C in chapter 3. This study would provide better insights into natural processes in Earth's surfaces such as weathering and diagenesis. We also discuss the relationship between structural changes in atomic scale and phase stability

in low temperature. Third, we explore the effect of iron content on structures (degree of polymerization and network connectivity) and the extent of disorder in iron-bearing sodium silicate glasses and melts utilizing Raman and high-resolution multi-nuclear ($^{29}$Si and $^{17}$O) solid-state NMR spectroscopy in chapter 4. Finally, appendix (abstract of papers participated and curriculum vitae) are presented in the end of this thesis.

Keyword: aluminum oxyhydroxide, low-temperature phase transition, Fe-bearing sodium silicate glass, NMR, $T_1$ relaxation, atomic structure

## 2. The principle of NMR

The nuclear magnetic resonance (NMR) phenomenon is based on the fact that nuclei of atoms have magnetic properties that can be utilized to yield chemical information. Quantum mechanically subatomic particles (protons, neutrons and electrons) have spin. In some atoms (e.g., $^{12}C$, $^{16}O$, $^{32}S$), these spins are paired and cancel each other out so that the nucleus of the atom has no overall spin. However, in many atoms ($^{1}H$, $^{13}C$, $^{31}P$, $^{15}N$, $^{19}F$, etc.) the nucleus does possess an overall spin.

In quantum mechanical terms, the nuclear magnetic moment of a nucleus will align with an externally applied magnetic field of strength **B0** in only 2I+1 ways, either with or against the applied field **B0** (Zeeman effect). For a single nucleus with I=1/2 and positive γ (gyromagnetic ratio), only one transition is possible between the two energy levels. The energetically preferred orientation has the magnetic moment aligned parallel with the applied field (spin m=+1/2), whereas the higher energy anti-parallel orientation (spin m=-1/2) also exist. The rotational axis of the spinning nucleus cannot be orientated exactly parallel (or anti-parallel) with the direction of the applied field **B0** but must precess about this field at an angle. Each nucleus has a characteristic value of γ, which is defined as a constant of proportionality between the nuclear angular momentum and magnetic moment. For a proton, $\gamma = 2.674 \times 10^4$ gauss$^{-1}$ sec$^{-1}$. This precession process generates an electric field with frequency $\omega_o$ (precession rate which is also called Larmor frequency). If we irradiate the sample with radio waves (in the MHz frequency range) the nucleus will absorb the energy

and be promoted to the less favorable higher energy state. This energy absorption is called resonance because the frequency of the applied radiation and the precession coincide or resonate. By irradiating the nucleus with electromagnetic radiation of the correct energy, a nucleus with a low energy orientation can be induced to transition to an orientation with a higher energy. The absorption of energy during this transition forms the basis of the NMR method.

A nuclear spin, however, experiences a great number of interactions in condensed matter such as solid phase. The main three interactions are dipolar coupling (interaction between magnetic moments of nuclei), chemical shift anisotropy (interaction between nuclear-electron interaction), and quadrupolar coupling (interaction between a nuclear electric quadrupole moment and an electric field gradient). These interactions often lead to very broad and featureless line. In liquids, most of these interactions will average out due to the rapid time-averaged molecular motion that occurs. Hence, it is necessary in solid-state NMR to apply techniques to achieve high resolution in spectra. These three interactions can be averaged by magic angle spinning (MAS) technique. The MAS NMR spectrum become narrower than static NMR spectrum and increasing the resolution for better identification and analysis by spinning the sample at the magic angle (=54.74°) with respect to the direction of the magnetic field. The nuclear dipole-dipole interaction averages to zero at magic angle. The chemical shift anisotropy also averages to a non-zero value. The quadrupolar interaction is only partially averaged by MAS leaving a residual secondary quadrupolar interaction.

One of the reasons for the impact of nuclear magnetic resonance on physics, chemistry, material science, and geology is its ability to give information about processes at the atomic level such as coordination number, bond length and angle distribution, and short–range ordering in atomic structure. In addition, solid-state NMR is an element specific and quantitative probe of short-range structure and thus suitable and powerful spectroscopy to investigate atomic configuration and extent of disorder in crystalline solid and amorphous oxide including silicates.

# 3. Atomistic origins of phase transition mechanism of aluminum (oxy)hydroxide polymorphs at low temperature: Insights from high resolution $^{27}$Al MAS NMR study

## 3.1. Introduction

The detailed knowledge of the atomic configuration changes of aluminum hydroxide and (oxy)hydroxide is essential for understanding diverse geological processes in the Earth's surfaces, such as weathering and diagenesis. Dehydroxylation and phase transition from aluminum (oxy)hydroxide to transition alumina at low temperature below 300°C is similar to the structural changes in layer silicates during burial diagenesis (e.g. smectite-illite transition). The study of structural transition occurring in simple aluminum (oxy)hydroxide thus allows getting better understanding of natural processes involving diverse metastable phases at low temperature. However, the detailed temperature-induced structural changes of aluminum (oxy)hydroxide polymorphs below 300°C is not fully understood. This is due mainly to a great variety of parameters such as time, transformation mechanism, and nature of starting materials, as well as the variables, such as temperature, pressure and composition, that are commonly used to define equilibrium in low temperature (Essene and Peacor, 1995). The objective of this study is to investigate the temperature-induced structural changes of varying aluminum (oxy)hydroxide polymorphs in well-designed experiment condition below 300°C using

high-resolution solid-state $^{27}Al$ MAS NMR.

Aluminum is the third most common element in Earth's crust and key component to form aluminum hydroxide, oxyhydroxide and alumina during weathering, hydration, and diagenesis in Earth's surface (Damodaran et al., 2002; Isobe et al., 2003; Levin and Brandon, 1998). Aluminum oxyhydroxide which is composed with aluminum, oxygen and hydroxyl has two different crystalline forms, boehmite (γ-AlOOH) and diaspore (α-AlOOH) in nature. Aluminum hydroxide also has two different crystalline forms, gibbsite (γ-$Al(OH)_3$) in nature and bayerite (α-$Al(OH)_3$) by synthesis.

Industrially, aluminum (oxy)hydroxide is one of the most important material. Aluminum (oxy)hydroxide polymorphs compose the bauxite which is aluminum ore and main provider of aluminum. Alumina, which is produced by annealing of aluminum (oxy)hydroxide, is most commonly used for catalysis and catalyst supports due to its thermal, chemical, and mechanical stability (Kim et al., 2007; Kwak et al., 2008; Paglia et al., 2004). Recently, aluminum (oxy)hydroxide also used of absorbent in pharmaceutical industry and mock marble in construction industry.

These aluminum (oxy)hydroxide polymorphs are a structural precursor of α-$Al_2O_3$ which has a well-known corundum structure at a higher temperature than 1200°C with each different thermal dehydroxylation and/or phase transition sequences for each aluminum (oxy)hydroxide polymorphs. It occurs in the following transformation sequences:

Boehmite (γ-AlOOH) $\longrightarrow$ γ $\longrightarrow$ δ $\longrightarrow$ θ $\longrightarrow$ α-$Al_2O_3$

Gibbsite (γ-$Al(OH)_3$) → boehmite $\longrightarrow$ γ $\longrightarrow$ δ $\longrightarrow$ θ $\longrightarrow$α-$Al_2O_3$

$\longrightarrow$ χ $\longrightarrow$ κ $\longrightarrow$ α-$Al_2O_3$

Bayerite (α-$Al(OH)_3$) $\longrightarrow$ η $\longrightarrow$ θ $\longrightarrow$ α-$Al_2O_3$

Irreversible dehydroxylation and phase transition of each aluminum (oxy)hydroxide polymorphs produces a series of metastable phases so-called transition aluminas (Hill et al., 2007; O'Dell et al., 2007; Pecharroman et al., 1999). Due to its metastability, transition alumina has wide range of phase transition temperature and co-exist with varies phases at same temperature. In particular, the detailed studies for dehydroxylation and phase transition in relatively low temperature still remains to be explored. This is because these processes are controlled by both thermodynamic and kinetic factors (Essene and Peacor, 1995), and thus well-constrained experiment is difficult. The investigation of structural changes is also difficult due to fine level of structural changes in low temperature.

Extensive research has been reported over the past few decades characterizing the structural changes in respect to dehydration and phase transformation. However, poorly developed and disordered crystallinity made it difficult to probe such fine and disordered structural changes using classic methods. In particular, X-ray diffraction (XRD) (Boumaza et al., 2009;

Zhou and Snyder, 1991) provides similar patterns for various phases and does not allow to unambiguously characterizing the phases because these structures have very similar d-spacing, which makes difficult the precise solution of the structure by XRD. Transmission electron microscopy (TEM) can clarify some of these problems, but, its spatial resolution is not adapted for providing a general description of samples. Infrared spectroscopy (IR) (Pecharroman et al., 1999), a representative method to identify unique vibrational modes of hydroxyl groups and bending and stretching modes $AlO^n$ polyhedra, has been used to prove the hydrogen environment of aluminum (oxy)hydroxides with increasing temperature. However, generally, those features were not fully resolved and cannot detect fine structure in low temperature. Achieving good resolution and quantification is essential to understanding of temperature-induced structural changes for varying aluminum (oxy)hydroxide polymorphs.

High-resolution solid-state NMR spectroscopy yields information that is element specific and allows the determination of short-range structures around elements of interest in diverse amorphous and disordered silicate (references). In particular, $^{27}Al$ MAS NMR spectroscopy is suited to characterize the coordination of aluminum and distortions of polyhedra with increasing temperature. However, there are some ambiguities to quantify the aluminum coordination in $^{27}Al$ MAS NMR spectra due to quadrupolar line broadening in previous study. Recent progress in solid-state NMR techniques including triple quantum magic angle spinning (3QMAS) NMR has yielded two-dimensional (2D) spectra, resolving structural details around quadrupolar nuclides. However, low

sensitivity of 2D NMR techniques precludes the detection of trace levels of aluminum coordination changes in low temperature. Thus, high-resolution $^{27}$Al MAS NMR spectrum is obtained to resolve structural details around quadrupolar nuclides at 11.7 T, obtaining a high signal-to-noise ratio by averaging of large number of $^{27}$Al MAS NMR spectrum.

Here, we explore the detailed temperature-induced structural changes below 300°C in aluminum (oxy)hydroxide polymorphs (boehmite, gibbsite, and bayerite) using high-resolution solid-state $^{27}$Al MAS NMR. These provide an insight into the dehydroxylation and phase transition mechanism for aluminum (oxy)hydroxide polymorphs. We also discuss difference of structural stabilities each phase depending on its initial precursor with comparison of the trend of temperature-induced structural changes.

### 3.2. Experimental procedure

**Sample preparation and characterization**

Boehmite and bayerite were synthesized by hydrolysis of aluminum tri-sec butoxide (ASB, Aldrich Chemical Co.). Boehmite was prepared by adding 4.52 g of ASB to 1.04 ml of distilled water which was dried for a week at room temperature (25°C) in air. For synthesizing of bayerite, ASB (5.23 g) was added to distilled water (200 ml). Gibbsite (99.7% of $Al(OH)_3$, $D_{50}$: 50 μm) was obtained from KC cooperation of Korea and was used as received. To confirm these three kinds of aluminum

(oxy)hydroxide polymorphs, we collected X-ray diffraction patterns of samples (Figure 1). X-ray diffraction spectra were collected on a X-ray diffractometer (using Cu Kα source (λ=1.5418 Å) in continuous mode between 2θ value of 10° and 70°, with a step size 0.01°/s. These samples were annealed for 2 h across the range of 50 ~ 300°C at 50°C increments using heating mantle and furnace with Pt crucible in air.

**NMR spectroscopy**

$^{27}$Al MAS NMR spectra for series of each aluminum (oxy)hydroxide polymorphs were collected at two static magnetic fields on Bruker Avance II 500 MHz (11.7 T) spectrometer with Larmor frequency of 130.28 MHz and 4 mm $ZrO_2$ rotor in triple-resonance MAS probe and on Varian 600 MHz spectrometer (14.1 T) at a Larmor frequency of 156.34 MHz using 2.5 mm $ZrO_2$ rotor in double-resonance MAS probe. The recycle delay was 1 s with radio-frequency pulse lengths of 0.23 μs (11.7 T) and 0.25 μs (14.1 T) which corresponds to about a 15° tip angle for the central transition in solids. Sample spinning speed was 15 kHz for 11.7 T and 20 kHz for 14.1 T. All spectra were referenced to $AlCl_3$ solution.

### 3.3. Results and Discussion

Figure 1 shows three different crystal structures for aluminum oxyhydroxide and hydroxide polymorphs. In the structure of boehmite (Figure 2A) (Walter and Oldfield, 1989), equivalent aluminum octahedra

([6]Al) are formed by coordination of Al to nonequivalent oxygen, and these octahedral are set out in straight double chains to build a sheetlike structure linked through hydrogen bonds between hydroxyls in neighboring planes. However, there are two crystallographically inequivalent aluminums that build layers of edge-sharing aluminum octahedra to produce the stacked layer sequence AB BA AB … (gibbsite, Figure 2B) (Saalfeld and Wedde, 1974) and AB AB AB … (bayerite, Figure 2C) (Zigan et al., 1978). These differences of crystal structure for aluminum octahedra can be resolved in $^{27}$Al MAS NMR spectrum of aluminum oxy-hydroxide polymorphs in Figure 3. $^{27}$Al MAS NMR spectra at 11.7 T of boehmite (Figure 3A) shows the presence of equivalent [6]Al site with single Gaussian curve at ~ 9.5 ppm. The spectra for gibbsite and bayerite (Figure 3B and 3C), however, present two distinct [6]Al sites. The spectrum of gibbsite (Figure 3B) consists of two lines, one with second-order quadrupolar structure, is known from previous studies (Bastow et al., 1994). For bayerite, observed chemical shifts of the peaks are 12.4 and 8.5 ppm. The two distinct [6]Al environments in gibbsite and bayerite show striking dissimilarity in the way chemical shielding and quadrupole interaction parameter are affected by the difference in the inequivalent [6]Al sites.

The $^{27}$Al MAS NMR spectra at 11.7 T for boehmite, gibbsite and bayerite series annealed at 50°C intervals from room temperature to 300°C are shown in Figure 4. As annealing temperature increases, the peak shapes and position of $^{27}$Al MAS NMR spectra vary with the atomic environment around aluminum, such as [4]Al, [5]Al and [6]Al. To clarify understanding the detailed structural transition changes, each spectrum was magnified 10

times in Figure 5. The spectra for boehmite series (Figure 4A and 5A) show the presence of $^{[4]}$Al and $^{[5]}$Al with increasing annealing temperature. The spectrum consists of three features at ~ 10, ~ 35, and 70 ppm, due to $^{[6]}$Al, $^{[5]}$Al, and $^{[4]}$Al. With increasing temperature, $^{[4]}$Al and $^{[5]}$Al fraction increase gradually even if annealing temperature is lower than 300°C, lower limit of structural transition temperature range from boehmite to γ-$Al_2O_3$. It is considered as a result of the disordered nature of the boehmite framework. This result, however, indicates the transition to γ-$Al_2O_3$ as also suggested by the previous $^{17}$O 3QMAS NMR result for presence of oxygen coordinated to three aluminum ions ($OAl_3$) under 300°C. According to these results, the phase transition temperature range would be expanded to lower temperature than 300°C.

The feature of $^{[5]}$Al also observed in only boehmite series with increasing temperature (Figure 5A). However, there are some uncertainties to ensure the presence of $^{[5]}$Al sites due to quadrupolar broadening cause of overlapping among $^{[n]}$Al feature in low field NMR. Therefore, high field NMR experiment needs to confirm the presence of $^{[5]}$Al sites. Figure 6 shows the $^{27}$Al MAS NMR spectra for boehmite series at 14.1 T. The feature of $^{[5]}$Al site is certainly resolved in 14.1 T. This yields unambiguous experimental evidence for the existence of $^{[5]}$Al sites in boehmite series although this fraction is relatively small. The presence of $^{[5]}$Al in boehmite series is significant to estimating the origins of structural stability which is noticeably lower than another polymorphs series. There are some controversy about the reason why $^{[5]}$Al exist, such as tentatively assigned to Al the external surface of alumina particle (Pecharroman et al., 1999) or

indicator disorder. Recently, the NMR experiment result suggests that $^{[5]}$Al can be regarded as the degree of disorder in the amorphous oxides, which increases with increasing $^{[5]}$Al contents and also the significant fractions (~ 40%) of $^{[5]}$Al in amorphous thin films suggest that amorphous $Al_2O_3$ may be potentially useful as a new class of catalysts (Lee et al., 2009). Thus, the presence or $^{[5]}$Al in boehmite suggest a larger topological disorder and may be responsible for gradual structural changes. The catalytic ability of γ-$Al_2O_3$ also can be explained on the presence of $^{[5]}$Al.

While the fraction of $^{[4]}$Al and $^{[5]}$Al increases gradually in boehmite series, the fraction of $^{[4]}$Al abruptly increases with increasing temperature in gibbsite and bayerite series. As will be discussed, there are no evidence to substantiate the presence of $^{[5]}$Al in gibbsite and bayerite series, implying the degree of disorder in atomic structure of boehmite series is extremely high. Figure 4B and 5B present the $^{27}$Al MAS NMR spectra for gibbsite series with increasing temperature. As mentioned above, the subsequent alumina phase formed by transition from gibbsite is γ-$Al_2O_3$ and χ-$Al_2O_3$. At this point a χ-$Al_2O_3$ component is non-detectable in XRD patterns so that it can be expected that the subsequent alumina phase is γ -$Al_2O_3$ in this study. The fraction of $^{[4]}$Al starts to increase slightly from 250°C and abruptly increases at 300°C, indicating the lower limit of structural transition temperature range is higher than boehmite series. Thus, this result shows the trend of structural transition in gibbsite series is totally different with boehmite series even if boehmite and gibbsite has same transition sequence to γ-$Al_2O_3$. This is due to difference of temperature-induced structural stability in between γ-$Al_2O_3$ formed from boehmite and

gibbsite. Thus, the γ-$Al_2O_3$ formed from gibbsite has higher structural stability than γ-$Al_2O_3$ formed from boehmite. It suggests that most important structural and textural properties of subsequent alumina formed downstream are strongly influenced by the phase of aluminum oxyhydroxide precursors.

Figure 4C and 5C shows the $^{27}Al$ MAS NMR spectra for bayerite series with increasing temperature. On heating, bayerite transforms to η-$Al_2O_3$ at 200 ~ 300°C, whereas boehmite and gibbsite transform to γ-$Al_2O_3$. The fraction of $^{[4]}Al$ starts to detect at 200°C, and abruptly increases at 250°C with faster increasing trend more than gibbsite series. And then, the fraction of $^{[4]}Al$ at 300°C is almost equal to at 250°C, implying phase transformation is already completed in 200 ~ 300°C. Compared with the transformation series of another aluminum hydrate polymorph, the transition temperature range of bayerite series is narrow. Thus, η-$Al_2O_3$ is more stable and less metastable than γ-$Al_2O_3$ in low temperature.

The peak width (full-width half-maximum, FWHM) of $^{[6]}Al$ measures the magnitudes of quadrupolar interactions and thus the degree of distortion around the Al coordination environments, such as bond length and bond angle. The peak width of $^{[6]}Al$ increases with increasing temperature in every aluminum oxyhydroxide polymorph series. This result indicates that the degree of Al site distortion increases due to formation of transition alumina which is metastable phase with increasing temperature. The trend of increasing peak width with increasing temperature is almost same with trend of Al coordination change. Thus, the degree of structural stability for the subsequent alumina from each

aluminum (oxy)hydroxide polymorphs can be estimated from the trend of Al coordination and peak width.

The quantification of fraction of $^{[4,5]}$Al is obtained by fitting $^{27}$Al MAS NMR spectra with multiple Gaussian function. The accurate and precise quantification of the Al coordination is not straightforward because of the asymmetric peak shape for the different Al coordination and the low concentration of $^{[4,5]}$Al for investigated temperature range. In order to extract quantitative data from the spectra, we applied the following fitting procedure. The total area of each $^{27}$Al MAS NMR spectrum was obtained, and then the peak of $^{[6]}$Al is fitted by three Gaussian components to account for the asymmetry of the peak and their combined area is considered to represent the abundance of $^{[6]}$Al. The next step is to subtract obtained $^{[6]}$Al abundance by fitting with three Gaussian function from total area. These values are abundance of $^{[4,5]}$Al for each spectrum. The uncertainties during this stage can lead to both random and systematic errors in the quantification of $^{[6]}$Al. We estimate the uncertainties on the abundances to be around 5% absolute.

Figure 7 shows distinct structural change behavior with different precursors using the variation in the fraction of $^{[4,5]}$Al in aluminum (oxy)hydroxide polymorphs with increasing temperature. The fraction of $^{[4,5]}$Al is normalized to the fraction of $^{[4,5]}$Al at 300°C for each aluminum (oxy) hydroxide polymorph. Figure 8 presents the $^{27}$Al MAS NMR spectra for all precursors annealed at 250°C, suggesting that the increasing $^{[4,5]}$Al fraction is distinct, and thus the degree of structural changes is also distinct with different precursors even at same temperature. Normalized population of

$^{[4,5]}$Al at 250°C by the fraction of $^{[4,5]}$Al at 300°C is 0.97 for bayerite, 0.82 for boehmite, and 0.21 for gibbsite, implying that structural changes is almost done for bayerite and is just started for gibbsite at 250°C. These distinct structural transition behavior is closely related to structural stability for each aluminum (oxy)hydroxide polymorph and subsequent alumina phases.

### 3.4. Conclusion

In this study, we explored the detailed temperature-induced structural change in aluminum (oxy)hydroxide polymorphs below 300°C using $^{27}$Al MAS NMR at 11.7 T and 14.1 T. The spectra show the evidence for the structural phase transition from aluminum (oxy) hydroxide polymorphs to transition alumina phase including γ-$Al_2O_3$ and η-$Al_2O_3$, the fraction of $^{[4]}$Al and peak widths of $^{[6]}$Al in aluminum (oxy)hydroxide polymorphs increase with increasing temperature. The detailed structural transition, however, shows distinct transition behavior. The presence of $^{[5]}$Al in boehmite and its absence in other polymorphs suggest a larger topological disorder in the former and may be responsible for gradual structural transitions. This result suggests that structural changes of aluminum (oxy) hydroxide depend on precursor minerals as well as temperature. The results provide the atomistic link to the structural phase transition of complex and heterogeneous natural materials, such as clay minerals in Earth's surface.

# 4. The effect of iron contents on structure and disorder in iron-bearing silicate glasses: High-resolution $^{29}Si$ and $^{17}O$ MAS and $^{17}O$ 3QMAS NMR

## 4.1. Introduction

The nature of polymerization or connectivity among framework cations and non-network cations and the extent of chemical and topological disorder in silicate glasses and melts is a key factor that affects their macroscopic thermodynamic and transport properties (e.g., energy, entropy, viscosity, diffusivity, crystal-melt partitioning coefficients, and activity coefficients of silica) and dynamics of magmas and partial melts in the Earth's crust and interior. They also allow us to understand geochemical processes involving magma (i.e., melting, migration, and emplacement) and have implications for the chemical differentiation of the early Earth. In particular, the iron in silicate glasses and melts also affect significantly their macroscopic properties. Understanding the structure and disorder of iron-bearing silicate glasses and melts provides constraints for the establishment of thermodynamic and transport model in tholeiitic magmas and iron-rich silicate system in core-mantle boundary. For example, liquid immiscibility is a well-known feature of alkaline-rich silicate liquids containing FeO. The $K_2O$-FeO-$Al_2O_3$-$SiO_2$ melts separate into Fe-rich mafic liquid and K-rich felsic liquid at low temperature (Roedder, 1951), suggesting that the coexistence of $Fe^{2+}$ and $K^+$ is energetically

unfavorable. Despite the importance and implications, the detailed structure and disorder in iron-bearing silicate glasses and melts are not fully understood.

Due to its ubiquitous abundance on Earth and its heterovalent nature in silicate melts and glasses, iron plays a significant role in many magmatic processes and iron redox-ratio ($Fe^{3+}/Fe^{2+}$) also affect to a wide number of physical and chemical properties of iron-bearing silicate glasses and melts system. The iron content affect the melt viscosity significantly. And the viscosity of iron-bearing silicate melts decrease considerably with decreasing $Fe^{3+}$ content of the melts (Bouhifd et al., 2004; Dingwell, 1989, 1991; Dingwell and Virgo, 1987; Liebske et al., 2003). Crystallization and melting behavior are also affected by iron contents and iron redox ratio of silicate melts and glasses (Carmichael and Ghiorso, 1986, 1990; Fudali, 1965; Shi and Libourel, 1991; Snyder et al., 1993; Toplis and Carroll, 1996; Toplis and Corgne, 2002; Wager, 1956). Hence, many studies have addressed structure role of $Fe^{3+}$ and $Fe^{2+}$ in melts and glasses (Alberto et al., 1996; Burkhard, 2000; Calas and Petiau, 1983; Galoisy et al., 2001; Giuli et al., 2002; Mysen and Virgo, 1985; Rossano et al., 1999; Rossano et al., 2000; Virgo and Mysen, 1985). The structural role of $Fe^{3+}$ in silicate melts and glasses in considered to be similar to that of Al. Thus, in most cases, $Fe^{3+}$ was assigned to tetrahedral site geometry, although evidence for higher coordination was also found, especially at low $Fe^{3+}$ contents (Farges et al., 2004; Hannoyer et al., 1992). On the other hand, $Fe^{2+}$ is distributed over sixfold-, fivefold- and fourfold-coordinated sites in silicate glasses and melts. The observation of fourfold $Fe^{2+}$ has been taken as evidence for

network-forming role of $Fe^{2+}$ (Jackson et al., 1993; Waychunas et al., 1988). However, a network-forming behavior of $Fe^{2+}$ is in conflict with viscosity data. In addition, the network-modifying role of $Fe^{2+}$ via redox-dependent changes in the polymerization of the samples was clearly shown using Raman spectroscopy (Wang et al., 1993, 1995).

Several decades of intense spectroscopic and diffraction studies have demonstrated that the short- and medium-range order of iron-bearing silicate glasses and melts strongly influences their bulk properties (Lee and Stebbins, 2002; McMillan and Wolf, 1995; Mysen, 2006; Navrotsky, 1995). In particular, Raman spectroscopy was utilized to study for iron-bearing silicate glasses (Mysen et al., 1985b; Virgo and Mysen, 1985; Wang et al., 1993, 1995).

However, no direct investigation of the local structure. Mossbauer spectroscopy (Burkhard, 2000; Mysen, 2006; Mysen et al., 1985a; Rossano et al., 2008; Virgo and Mysen, 1985) is common technique to investigate iron redox ratio and structural roles, but those features were not fully resolved. The iron 1s-3d pre-edge features have been investigated as a function of the oxidation state and coordination geometry of iron in silicate glasses and melts using XANES method (Bonnin-Mosbah et al., 2001; Brown et al., 1995; Delaney et al., 1998; Galoisy et al., 2001; Wilke et al., 2007; Wilke et al., 2001) but the connectivity and polymerization of iron-bearing silicate glasses cannot be yielded directly.

Advanced in modern high-resolution solid-state NMR methods provide new opportunities in the study the glass structure and disorder. Because NMR can provide element-specific atomic configurations around

nuclide of interest, it is particularly suitable to study for environments around multi-nuclear. However, there is critical problem to investigate atomic structure and disorder of iron-bearing silicate glasses using solid-state NMR spectroscopy due to paramagnetic properties of iron.

The paramagnetic properties of iron seriously limit the application of solid-state NMR spectroscopy for the iron-bearing silicate glasses and melts. Unpaired electrons in paramagnetic cation such as iron, nickel, and manganese give rise to strong local magnetic fields that mask original spectroscopic properties of objects investigated, such as chemical shift, signal loss, line shapes of resonances, and their $T_1$ (spin-lattice relaxation), $T_2$ (spin-spin relaxation) relaxation times (Kelsey et al., 2008; Sharp et al., 2001; Stebbins and Kelsey, 2009). For example, early reports showed severe broadening of $^{29}$Si MAS NMR peaks, and even loss of an observable signal, in minerals such as olivine ($[Mg,Fe]_2SiO_4$) with a few wt% FeO (Grimmer et al., 1983; Smith et al., 1983). $^{29}$Si MAS NMR spectrum for natural samples of pyrope garnet ($[Mg,Fe]_3Al_2Si_3O_{12}$), containing up to 3.5 wt% FeO (Stebbins and Kelsey, 2009), and olivine polymorphs with cobalt impurities (Stebbins et al., 2009) contain anomalous NMR peaks which would be considered by pseudo-contact shifts from dipolar interactions with unpaired electron spins. Thus, generally, the presence of paramagnetic cations in solids is not desirable, particularly at accurate structural studies of materials by NMR.

Influence of paramagnetic cations, however, will obviously depend on their concentrations and electron relaxation times. The term "relaxation" is widely used in the physical sciences to indicate the re-establishment of thermal equilibrium after some perturbation is applied. Thermal

equilibrium is first established in the absence of a field, so that all nuclear spin orientations are equally likely. When a magnetic field is applied, this situation no longer corresponds to equilibrium, and the system relaxes to the new equilibrium state, in which the spin polarizations are distributed anisotropically. If the magnetic field is suddenly switched off at later time $t_{off}$ (where $t_{on}$-$t_{off}$>>$T_1$), the nuclear spin magnetization relaxes back to zero again (Bakhmutov, 2011). The relaxation time constant $T_1$ depends on the nucleus and the sample, indicating parameters such as temperature and viscosity, if the sample is liquid. Typically, the value of $T_1$ is in the range ms to s, although $T_1$ may be as long as days or even years in exceptional cases. However, this $T_1$ relaxation time is significantly shortened due to paramagnetic cations. The $T_1$ relaxation time is controlled by recycle delay in solid-state NMR experiment. Therefore, their optimal combinations can lead to a number of positive effects. In general, signal-to-noise (S/N) ratio of NMR signal is decrease for iron-bearing materials, but S/N ratio is developed by averaging of a lot of scanning of signals due to short recycle delay time. Thus, we can obtain high-resolution solid-state NMR spectra for direct investigation of the local structure and disorder in iron-bearing silicate glasses in spite of paramagnetic cation.

$^{29}$Si MAS NMR is one of the most well-established solid-state NMR techniques for probing the environment around Si atom in silicate materials (Duxson et al., 2005; Kirkpatrick et al., 1986; Lee and Stebbins, 1999; Pierce et al., 2010). The environment around Si atom can be described using $Q^n$ notation which refers to tetrahedral Si groups with n number of bridging oxygen atoms.

$^{17}$O NMR is unique probe of local structures around bridging and non-bridging oxygen (BO and NBO) that can provide critical information on the extent of disorder among framework and non-framework cation (e.g., connectivity, degree or polymerization, non-framework disorder, topological disorder, etc.). While conventional $^{17}$O MAS NMR often cannot yield highly resolved spectra due to residual second order quadrupolar broadening, in these studies 2D (dimensional) $^{17}$O 3QMAS NMR provides significantly improved resolution over MAS NMR and has been applied to a diverse range of oxide glasses quenched from melts (Allwardt and Stebbins, 2004; Du and Stebbins, 2003; Lee, 2005; Lee et al., 2004; Lee et al., 2010a; Lee and Stebbins, 2009). $^{17}$O 3QMAS NMR studies allow us to probe the detailed bonding environments around the bridging (BO) and non-bridging oxygens (NBOs), and thus provide quantitative estimates of the degree of cation mixing among framework and non-framework cation in silicate glasses system.

Here, we report the first high-resolution solid-state NMR spectra ($^{29}$Si and $^{17}$O) for iron-bearing sodium silicate glasses, together with Raman spectra. Sodium silicate glasses and melts are archetypal model systems for assessing new approaches to understanding structural investigation for complex covalent oxide glasses and melts. This system has key implications for geochemical processes such as magma dynamics and melts generation in subduction zones as well as wide applications in the glass and ceramic industry, stimulating extensive studies of their atomic structures with various spectroscopic and scattering techniques (Angeli et al., 2010; Lee et al., 2009; Malfait et al., 2008; Stebbins et al., 1995). In addition, sodium

silicate glasses are the ideal system to study atomic structure in silicate melts due to their relatively low liquidus temperature and wide glass forming region. These provide an insight into the effect of iron content on structure (polymerization and connectivity) and extents of disorder in iron-bearing sodium silicate glasses, model system for complex magma. We also discuss the structural role of iron in the silicate glasses.

## 4.2. Experimental Procedure

### Sample preparation and characterization

Sodium disilicate and iron-bearing sodium silicate glasses with varying $Fe_2O_3$ contents (see Table 1.) [e.g., $(Na_2O)_{1-x}\cdot(Fe_2O_3)_x\cdot(SiO_2)_2$ with x=0.03, 0.05, 0.10, 0.20, 0.30, 0.50] were synthesized from sodium carbonate ($Na_2CO_3$) and oxide reagents ($Fe_2O_3$ and $SiO_2$). For $^{17}O$ MAS and 3QMAS NMR experiment, 20% $^{17}O$-enriched $SiO_2$ was used to synthesize $(Na_2O)_{1-x}\cdot(Fe_2O_3)_x\cdot(SiO_2)_2$ with X=0.05, 0.10, 0.20. The 20% $^{17}O$-enriched $SiO_2$ was prepared by hydrolyzing $SiCl_4$ in 20% $^{17}O$-enriched water. For sodium disilicate, 0.2 wt% of cobalt oxide was added to reduce spin-lattice relaxation time. The mixtures in Pt crucible were decarbonated at 700°C for 1 h and fused at 1100°C for 1 h in an Ar environment. The melt was quenched by removing the Pt crucible from the furnace and manually lowering it into distilled water. To avoid iron loss through saturation of the used Pt crucible with Fe, glass synthesis process was repeated two times using same Pt crucible.

**NMR spectroscopy**

$^{29}Si$ MAS NMR spectra were collected on a Varian 400 MHz solid-state spectrometer (9.4 T) at a Larmor frequency of 79.48 MHz for $^{29}Si$ with a 4 mm $ZrO_2$ rotor in Doty Scientific triple-resonance magic-angle spinning (MAS) probe. The recycle delay was 60 s for iron-free sodium disilicate and 0.3~1 s for iron-bearing samples with the radio-frequency pulse lengths of 1.67 μs that correspond to about a 30° tip angle for the central transition in solid. The sample spinning speed was 14 kHz. The spectra were referenced to tetra-methyle silane (TMS).

We also collected $^{17}O$ MAS and 3QMAS NMR spectra for $(Na_2O)_{1-x}\cdot(Fe_2O_3)_x\cdot(SiO_2)_2$ with X=0.05, 0.10, and 0.20 at 9.4 T with 4 mm silicon nitride rotor in same probe. The recycle delay for MAS NMR experiment is 0.3 s, with radio-frequency pulse lengths of 0.3 us (about 15° tip angle for the central transition in solids). $^{17}O$ 3QMAS NMR spectra were collected using fast-amplitude modulation (FAM) based shifted-echo pulse sequences [5.5 μs –delay – 2 μs – echo delay (approximately 0.17 ms) – 20 μs]. The recycle delay is 1 s, and a spinning speed of 14 kHz was used. The $^{17}O$ NMR spectra were referenced to external tap water.

**Raman spectroscopy**

The Raman spectra were obtained with Raman-laser spectroscopy built in Seoul National University, using the 488 nm line of an external argon laser with typically 50 mW of laser power at the sample surface. The spectra were collected with 40 acquisitions of 30 s each.

## 4.3. Results and Discussion

### 4.3.1. Effect of iron content on degree of polymerization: Raman spectroscopy results

Figure 9 shows the Raman spectra for iron-bearing sodium silicate glasses [$(Na_2O)_{1-x} \cdot (Fe_2O_3)_x \cdot (SiO_2)_2$] with varying iron content, $X_{Fe_2O_3}$ [$=Fe_2O_3/(Fe_2O_3+Na_2O)$]. There is a broad, asymmetry peak at 500 to 600 $cm^{-1}$. This peak is a composite peak due to bending vibrations of the silicate network and four-membered rings (McMillan and Hess, 1990). The overall peak decreases intensity and shifts to lower wavenumbers with increasing $Fe_2O_3$ content. At higher $Fe_2O_3$ contents, it is difficult to analyze due to peak broadening.

The remainder of this Raman experiment will focus on the spectral region between 850 and 1250 $cm^{-1}$. This is the region where the stretching vibrations of the different $Q^n$ species are present (indicated on Figure 9). In this spectra region, several changes occur with increasing $Fe_2O_3$ content. The peak, assigned to $Q^4$ (Mysen and Frantz, 1993b), is not resolved in these spectra. The position of the 1100 $cm^{-1}$ peak, which is generally assigned to $Q^3$ (McMillan et al., 1992; Mysen and Frantz, 1993a, b) decrease in intensity with increasing $Fe_2O_3$ content and seems to shifts to lower wavenumbers at higher $Fe_2O_3$ content. The peak at ~950 $cm^{-1}$, which can be unambiguously assigned to $Q^2$ (McMillan et al., 1992; Mysen and Frantz, 1993a) rapidly increases in intensity with increasing $Fe_2O_3$ content. The

weak shoulder around 850 $cm^{-1}$ is present at iron-free sodium disilicate. This peak, which can be assigned to $Q^1$ (McMillan and Wolf, 1995), also rapidly increase with increasing $Fe_2O_3$. However, it is difficult to imply that the degree of polymerization decrease with increasing iron content because the frequency of vibration of Fe-O is lower than Si-O. Thus, the peak shift may be considered in iron-bearing silicate glasses in these spectra.

### 4.3.2. Effects of iron contents on spin-lattice relaxation: 29Si T1 relaxation time measurements

Spin-lattice relaxation ($T_1$ relaxation) data presented hear based on saturation-recovery measurements. After a train of pulses to saturate the magnetization, an incremented time delay (**τ**) is allowed for partial recovery, and then an observed pulse is used to measure the signal (Stebbins and Kelsey, 2009). Directly integrated or fitted peak areas (M) were normalized to that observed in the longest-delay spectrum as an approximation of the fully relaxed value ($M_\infty$) and analyzed with a "stretched exponential" equation (Tse and Hartmann, 1968; Hartman et al., 2007).

$$M/M_\infty = A[1 - \exp[-(\tau/T')^\beta]]$$

Here, *A* is a constant that would be precisely 1 if the longest delay magnetization was exactly that of the fully relaxed sample; commonly relaxation may not be 100% complete so that *A* is slightly less than 1. *A* value of either less than or greater than 1 can result simply from fitting

imprecision as well. In cases where the magnetization equilibrates rapidly throughout the sample (for example by physical or spin diffusion), all spins may relax at the same rate and a single exponential behavior ($\beta = 1$) is commonly observed. In this case, T′ is equivalent to a single "spin-lattice relaxation time" $T_1$. However, it is common for $^{29}Si$ in silicate that relaxation is dominated by through-space dipolar coupling between nuclear spins and the unpaired electronic spins of paramagnetic cations. In this case, relaxation of each spin will depend strongly on the distance to an paramagnetic center. This heterogeneity often results in relaxation that is well-approximated by a "stretched" exponential with $\beta = 0.5$ (Tse and hartmann, 1968; Hartman et al., 2007; Hartman and Sherriff, 1991; Stebbins et al., 2009; Hayashi et al., 1992). In cases where mixed relaxation mechanisms are present, relaxation curves may be best fitted with values of $\beta$ between 0.5 and 1. Figure 10 and Figure 11 show that the $^{29}Si$ $T_1$ relaxation (saturation-recovery) time for iron-bearing sodium silicate glasses with varying $X_{Fe_2O_3}$ decrease with increasing iron content due to an enhanced interaction between nuclear spin and unpaired electron.

### 4.3.3. Signal intensity and spinning sideband of NMR spectra with increasing paramagnetic cation contents

Figure 12 shows $^{29}Si$ MAS NMR spectra for iron-bearing sodium disilicate glasses $[(Na_2O)_{1-x}\cdot(Fe_2O_3)_x\cdot(SiO_2)_2]$ with varying iron-content [$X_{Fe_2O_3}$=$Fe_2O_3$/($Fe_2O_3$+ $Na_2O$), 0, 0.03, 0.05, 0.10, 0.20, 0.30, 0.50]. Note that vertical scale of these spectra (Figure 12) is absolute value for comparison the peak intensity between each sample with varying $Fe_2O_3$ content. Three

distinct Si environments ($Q^n$ species) for $^{[4]}$Si are partially resolved in $^{29}$Si MAS spectra for iron-free sodium disilicate. The features relevant to $Q^2$ (~ -75 ppm), $Q^3$ (~ -90 ppm), and $Q^4$ (broad component ~ 100 ppm) species are revealed. The peak intensity of $^{29}$Si MAS NMR is exponentially decreases and the peak width is increase with increasing iron content. Thus, a single broad peak is observed in $^{29}$Si MAS NMR spectra for iron-bearing sodium silicate glasses with high $Fe_2O_3$ content. Figure 13 shows $^{17}$O MAS NMR spectra for iron-bearing sodium silicate glasses $[(Na_2O)_{1-x}\cdot(Fe_2O_3)_x\cdot(SiO_2)_2]$ with varying iron content [$X_{Fe_2O_3} = Fe_2O_3/(Fe_2O_3 + Na_2O)$, 0, 0.05, 0.10, 0.20]. The vertical scale of Figure 13 is also absolute value. The peak intensity of $^{17}$O MAS NMR spectra is also exponentially decreases with increasing iron content. As shown in Figure 14, the trend of signal loss is consistent between $^{29}$Si and $^{17}$O MAS NMR spectra with increasing iron content. In particular, the signal intensity of $^{29}$Si MAS NMR exponentially decreases with increasing iron content. This result is consistent with decreasing $^{29}$Si $T_1$ relaxation time with increasing iron content, implying that the enhanced interaction between nuclear spin and unpaired electron is led to decrease signal intensity. While the signal intensity decreases exponentially, signal is detected in MAS NMR even iron content is up to 34.60 wt% of $Fe_2O_3$.

Figure 15 and Figure 16 shows $^{29}$Si and $^{17}$O MAS NMR spectra for iron-bearing sodium silicate with varying iron content. These figures are equal to Figure 12 and 13 but horizontal scale is extended for observing of spinning sideband. While the signal intensity decreases exponentially, the decaying of spinning sideband intensity is distinct behavior with increasing iron content.

### 4.3.4. Effect of iron content on distribution of $Q^n$ species around Fe: $^{29}Si$ MAS NMR results

Figure 17 shows the $^{29}Si$ MAS NMR spectra for iron-bearing sodium disilicate glasses $[(Na_2O)_{1-x}\cdot(Fe_2O_3)_x\cdot(SiO_2)_2]$ with varying iron content $[X_{Fe_2O_3}=Fe_2O_3/(Fe_2O_3+ Na_2O)$, 0, 0.03, 0.05, 0.10, 0.20, 0.30, 0.50]. Three distinct Si environments, relevant to $Q^2$ (~ -75 ppm), $Q^3$ (~ -90 ppm), and $Q^4$ (broad component ~ 100 ppm) species, are partially resolved in $^{29}Si$ MAS spectra for iron-free sodium disilicate. However, a single broad peak is observed in $^{29}Si$ MAS NMR spectra for iron-bearing sodium silicate with higher than $X_{Fe_2O_3}=0.05$ due to peak broadening with increasing $Fe_2O_3$ content. Figure 18 shows that the peak widths (full-width at half-maximum, FWHM) of the $^{29}Si$ MAS NMR spectra for the iron-bearing sodium silicate glasses increase with increasing iron content from approximately 13 ppm for $X_{Fe_2O_3}$ =0.05 to approximately 23 ppm for $X_{Fe_2O_3}=0.50$. The trend of increasing peak width is diametrically the opposite of the trend of signal loss with increasing iron content (Figure 16). Thus, it is difficult to infer the changes in $Q^n$ species with increasing iron content using $^{29}Si$ MAS NMR spectra. The position of peak maximum increases with increasing $X_{Fe_2O_3}$ from -88.7 ppm for $X_{Fe_2O_3}=0$ to -93.2 ppm for $X_{Fe_2O_3}=0.5$, but the change of peak position is negligible.

### 4.3.5. Effects of iron contents on network connectivity and disorder in iron-bearing sodium silicate glasses: 17O MAS NMR and 3QMAS NMR results

The peak shapes and positions determined by chemical shift, $C_q$, and η in $^{17}O$ MAS and 3QMAS NMR spectra vary with the atomic environment around oxygen in silicate glasses. Thus these values are useful to understanding the effect of iron content on structure and disorder for iron-bearing silicate glasses and melts.

Figure 19 shows the $^{17}O$ MAS NMR spectra for iron-bearing sodium disilicate glasses $[(Na_2O)_{1-x}\cdot(Fe_2O_3)_x\cdot(SiO_2)_2]$ with varying iron content $[X_{Fe_2O_3}=Fe_2O_3/(Fe_2O_3+ Na_2O)]$ at 9.4 T. The MAS spectrum for iron-free sodium disilicate is consistent with previous results (Lee et al., 2009; Xue et al., 1994). While a NBO peak (a narrow component around 35 ppm, Na-O-Si) and a BO peak (a broad component, Si-O-Si) are partially resolved in $^{17}O$ MAS NMR spectra for the iron-free sodium disilicate glass. The peak width of NBO and BO peak in glasses clearly increase with increasing $Fe_2O_3$ content, consistent with increasing topological disorder (e.g., broadening of bond length and angle distribution). Thus, the NBO and BO peak are somewhat less well resolved for iron-bearing sodium silicate glasses with $X_{Fe_2O_3}$=0.05 and totally overlapped for $X_{Fe_2O_3}$=0.10 and 0.20, making it difficult to infer the changes in oxygen configuration with the increasing $Fe_2O_3$ content. Peak position of NBO peaks slightly shift toward lower frequency (more positive in frequency domain) with increasing $Fe_2O_3$ content. It is clear, however, that the peak shape and width vary with the $Fe_2O_3$ content, implying changes in oxygen cluster population and atomic environment around oxygen. In particular, the peak width of NBO for iron-bearing silicate glasses seems to be broader than BO with increasing $Fe_2O_3$ content. Whereas more resolution would be necessary to confirm its

assignment, peak broadening with increasing $Fe_2O_3$ content suggests that both NBO and BO environments are affected by iron and stronger interaction between iron and NBO sites than BO sites.

3QMAS NMR provides a much improved resolution in the two-dimensional (2D) spectra for quadrupolar nuclides (Amoureux et al., 1996; Frydman and Harwood, 1995; Medek et al., 1995) over one-dimensional MAS NMR and thus can yield detailed information on the network connectivity in oxide glasses (Dirken et al., 1997; Lee et al., 2009; Stebbins and Xu, 1997). Figure 20 shows $^{17}O$ 3QMAS NMR spectra for iron-bearing sodium silicate glasses with vary $X_{Fe_2O_3}$, yielding improved resolution among BO and NBO sites as labeled in Figure 20 over conventional MAS spectra (Figure 19). NBO (Na-O-Si, about -25 ppm in the isotropic dimension) and BO (Si-O-Si, -56 ppm in isotropic dimension) sites are fully resolved for iron-free sodium disilicate glass. NBO and BO peak for iron-bearing glasses, however, are partially resolved each oxygen cluster peaks due to peak broadening with increasing $Fe_2O_3$ content. The widths of both NBO and BO peaks in the isotropic dimension increase with increasing $Fe_2O_3$ content. Figure 21 presents the total isotropic projection of the 2D $^{17}O$ 3QMAS NMR spectra for iron-bearing sodium disilicate glasses with varying $Fe_2O_3$ content. The peak intensity, position, and width for each NBO and BO peak varies, indicating changes in structurally relevant NMR parameters and the degree of disorder with the with $Fe_2O_3$ content. The widths of the BO and NBO peaks abruptly increase with the $Fe_2O_3$ content.

### 4.4. Conclusion

In this study, we report the first experimental results on the effects of iron content on the structure and disorder of iron-bearing sodium silicate glasses (up to 34.60 wt% $Fe_2O_3$) using Raman and $^{29}Si$ and $^{17}O$ solid-state NMR spectroscopy. The $^{29}Si$ $T_1$ relaxation time and peak intensity decrease and peak broadening increases with increasing iron content due to enhanced interaction between nuclear spin and unpaired electron. The heterogeneous peak broadening in $^{29}Si$ and $^{17}O$ MAS NMR spectra suggests the heterogeneous distribution of $Q^n$ species and oxygen cluster (NBO and BO) around iron in iron-bearing silicate glasses. The $^{17}O$ 3QMAS NMR spectra for iron-bearing sodium silicate glasses show well-resolved NBO and BO sites even at varying iron content (up to 34.60 wt%). These results demonstrate that solid-state NMR, particular $^{17}O$ 3QMAS NMR can be effective probe the structure and disorder of iron-bearing silicate glasses. In this study, we reported the first experimental data to explore the structure and disorder in iron-bearing silicate glasses and melts using solid-state NMR, which can shed light on opportunities to study of effect of iron content on the element partitioning between crystals and melts in silicate glasses and melts as well as transport properties, such as viscosity. It also may provide an atomistic explanation for chemical reaction between silicate mantle and liquid metal core of partially molten iron-rich structure in core-mantle boundary, and thus can predict the thermal history of Earth and terrestrial planets, such as Mars.

## References


Alberto, H.V., daCunha, J.L.P., Mysen, B.O., Gil, J.M., and deCampos, N.A., 1996, Analysis of Mossbauer spectra of silicate glasses using a two-dimensional Gaussian distribution of hyperfine parameters: Journal of Non-Crystalline Solids, v. 194, p. 48-57.

Allwardt, J.R., and Stebbins, J.F., 2004, Ca-Mg and K-Mg mixing around non-bridging O atoms in silicate glasses: An investigation using O-17 MAS and 3QMAS NMR: American Mineralogist, v. 89, p. 777-784.

Amoureux, J.P., Fernandez, C., and Frydman, L., 1996, Optimized multiple-quantum magic-angle spinning NMR experiments on half-integer quadrupoles: Chemical Physics Letters, v. 259, p. 347-355.

Angeli, F., Charpentier, T., de Ligny, D., and Cailleteauz, C., 2010, Boron Speciation in Soda-Lime Borosilicate Glasses Containing Zirconium: Journal of the American Ceramic Society, v. 93, p. 2693-2704.

Bakhmutov, V.I., 2011, Strategies for Solid-State NMR Studies of Materials: From Diamagnetic to Paramagnetic Porous Solids: Chemical Reviews, v. 111, p. 530-562.

Bastow, T.J., Hall, J.S., Smith, M.E., and Steuernagel, S., 1994, Characterization of hydrated aluminas by MAS and DOR Al-27 NMR: Mater. Lett., v. 18, p. 197-200.

Bokhimi, X., Toledo-Antonio, J.A., Guzman-Castillo, M.L., Mar-Mar, B., Hernandez-Beltran, F., and Navarrete, J., 2001, Dependence of

boehmite thermal evolution on its atom bond lengths and crystallite size: Journal of Solid State Chemistry, v. 161, p. 319-326.

Bonnin-Mosbah, M., Simionovici, A.S., Metrich, N., Duraud, J.P., Massare, D., and Dillmann, P., 2001, Iron oxidation states in silicate glass fragments and glass inclusions with a XANES micro-probe: Journal of Non-Crystalline Solids, v. 288, p. 103-113.

Bouhifd, M.A., Richet, P., Besson, P., Roskosz, M., and Ingrin, J., 2004, Redox state, microstructure and viscosity of a partially crystallized basalt melt: Earth and Planetary Science Letters, v. 218, p. 31-44.

Boumaza, A., Favaro, L., Ledion, J., Sattonnay, G., Brubach, J.B., Berthet, P., Huntz, A.M., Roy, P., and Tetot, R., 2009, Transition alumina phases induced by heat treatment of boehmite: An X-ray diffraction and infrared spectroscopy study: Journal of Solid State Chemistry, v. 182, p. 1171-1176.

Brown, G.E., Farges, F., and Calas, G., 1995, X-ray scattering and x-ray spectroscopy studies of silicate melts, Structure, Dynamics and Properties of Silicate Melts, Volume 32: Reviews in Mineralogy, p. 317-410.

Burkhard, D.J.M., 2000, Iron-bearing silicate glasses at ambient conditions: Journal of Non-Crystalline Solids, v. 275, p. 175-188.

Calas, G., and Petiau, J., 1983, Coordination of iron in oxide glasses through high-resolution K-edge spectra - information from the pre-edge: Solid State Communications, v. 48, p. 625-629.

Carmichael, I.S.E., and Ghiorso, M.S., 1986, Oxidation-reduction relations

in basic magma - a case for homogeneous equilibria: Earth and Planetary Science Letters, v. 78, p. 200-210.

Carmichael, I.S.E., and Ghiorso, M.S., 1990, The effect of oxygen fugacity on the redox state of natural liquids and their crystallizing phases: Reviews in Mineralogy, v. 24, p. 191-212.

Damodaran, K., Rajamohanan, P.R., Chakrabarty, D., Racherla, U.S., Manohar, V., Fernandez, C., Amoureux, J.P., and Ganapathy, S., 2002, Triple-quantum magic angle spinning Al-27 NMR of aluminum hydroxides: J. Am. Chem. Soc., v. 124, p. 3200-3201.

Delaney, J.S., Dyar, M.D., Sutton, S.R., and Bajt, S., 1998, Redox ratios with relevant resolution: Solving an old problem by using the synchrotron microXANES probe: Geology, v. 26, p. 139-142.

Dingwell, D.B., 1989, Shear viscosities of ferrosilicate liquids: American Mineralogist, v. 74, p. 1038-1044.

Dingwell, D.B., 1991, Redox viscometry of some Fe-bearing silicate melts: American Mineralogist, v. 76, p. 1560-1562.

Dingwell, D.B., and Virgo, D., 1987, The effect of oxidation-state on the viscosity of melts in the system $Na_2O$-FeO-$Fe_2O_3$-$SiO_2$: Geochimica Et Cosmochimica Acta, v. 51, p. 195-205.

Dirken, P.J., Kohn, S.C., Smith, M.E., and vanEck, E.R.H., 1997, Complete resolution of Si-O-Si and Si-O-Al fragments in an aluminosilicate glass by O-17 multiple quantum magic angle spinning NMR spectroscopy: Chemical Physics Letters, v. 266, p. 568-574.

Du, L.S., and Stebbins, J.F., 2003, Nature of silicon-boron mixing in sodium borosilicate glasses: A high-resolution B-11 and O-17 NMR study: Journal of Physical Chemistry B, v. 107, p. 10063-10076.

Duxson, P., Provis, J.L., Lukey, G.C., Separovic, F., and van Deventer, J.S.J., 2005, Si-29 NMR study of structural ordering in aluminosilicate geopolymer gels: Langmuir, v. 21, p. 3028-3036.

Essene, E.J., and Peacor, D.R., 1995, Clay mineral thermometry - A critical perspective: Clays and Clay Minerals, v. 43, p. 540-553.

Farges, F., Lefrere, Y., Rossano, S., Berthereau, A., Calas, G., and Brown, G.E., 2004, The effect of redox state on the local structural environment of iron in silicate glasses: a molecular dynamics, combined XAFS spectroscopy, and bond valence study: Journal of Non-Crystalline Solids, v. 344, p. 176-188.

Frydman, L., and Harwood, J.S., 1995, Isotropic spectra of half-integer quadrupolar spins from bidimensional magic-angle-spinning nmr: Journal of the American Chemical Society, v. 117, p. 5367-5368.

Fudali, R.F., 1965, Oxygen fugacities of basaltic and andesitic magmas: Geochimica Et Cosmochimica Acta, v. 29, p. 1063-&.

Galoisy, L., Calas, G., and Arrio, M.A., 2001, High-resolution XANES spectra of iron in minerals and glasses: structural information from the pre-edge region: Chemical Geology, v. 174, p. 307-319.

Giuli, G., Pratesi, G., Cipriani, C., and Paris, E., 2002, Iron local structure in tektites and impact glasses by extended X-ray absorption fine structure and high-resolution X-ray absorption near-edge structure

spectroscopy: Geochimica Et Cosmochimica Acta, v. 66, p. 4347-4353.

Grimmer, A.R., Vonlampe, F., Magi, M., and Lippmaa, E., 1983, Solid-state high-resolution Si-29-NMR of silicates - influence of $Fe^{2+}$ in olivines: Zeitschrift Fur Chemie, v. 23, p. 343-344.

Hannoyer, B., Lenglet, M., Durr, J., and Cortes, R., 1992, Spectroscopic evidence of octahedral iron(III) in soda-lime silicate-glasses: Journal of Non-Crystalline Solids, v. 151, p. 209-216.

Hemingway, B.S., 1991, Thermodynamic properties of anthophyllite and talc - corrections and discussion of calorimetric data: American Mineralogist, v. 76, p. 1589-1596.

Hemingway, B.S., Robie, R.A., Evans, H.T., and Kerrick, D.M., 1991, Heat-capacities and entropies of sillimanite, fibrolite, andalusite, kyanite, and quartz and the $Al_2SiO_5$ phase-diagram: American Mineralogist, v. 76, p. 1597-1613.

Hill, M.R., Bastow, T.J., Celotto, S., and Hill, A.J., 2007, Integrated study of the calcination cycle from gibbsite to corundum: Chem. Mater., v. 19, p. 2877-2883.

Isobe, T., Watanabe, T., de la Caillerie, J.B.D., Legrand, A.P., and Massiot, D., 2003, Solid-state H-1 and Al-27 NMR studies of amorphous aluminum hydroxides: Journal of Colloid and Interface Science, v. 261, p. 320-324.

Jackson, W.E., Deleon, J.M., Brown, G.E., Waychunas, G.A., Conradson, S.D., and Combes, J.M., 1993, High-temperature xas study of

$Fe_2SiO_4$ liquid - reduced coordination of ferrous iron: Science, v. 262, p. 229-233.

Kelsey, K.E., Stebbins, J.F., Du, L.S., Mosenfelder, J.L., Asimow, P.D., and Geiger, C.A., 2008, Cation order/disorder behavior and crystal chemistry of pyrope-grossular garnets: An O-17 3QMAS and Al-27 MAS NMR spectroscopic study: American Mineralogist, v. 93, p. 134-143.

Kim, H.J., Lee, H.C., and Lee, J.S., 2007, Al-27 triple-quantum magic-angle spinning nuclear magnetic resonance characterization of nanostructured alumina materials: J. Phys. Chem. C, v. 111, p. 1579-1583.

Kirkpatrick, R.J., Oestrike, R., Weiss, C.A., Smith, K.A., and Oldfield, E., 1986, High-resolution Al-27 and Si-29 NMR spectroscopy of glasses and crystals along the join CaMgSi2O6-$CaAl_2SiO_6$: American Mineralogist, v. 71, p. 705-711.

Kwak, J.H., Hu, J.Z., Lukaski, A., Kim, D.H., Szanyi, J., and Peden, C.H.F., 2008, Role of pentacoordinated $Al^{3+}$ ions in the high temperature phase transformation of gamma-$Al_2O_3$: J. Phys. Chem. C, v. 112, p. 9486-9492.

Lee, S.K., 2005, Microscopic origins of macroscopic properties of silicate melts and glasses at ambient and high pressure: Implications for melt generation and dynamics: Geochimica Et Cosmochimica Acta, v. 69, p. 3695-3710.

Lee, S.K., Cody, G.D., Fei, Y.W., and Mysen, B.O., 2004, Nature of

polymerization and properties of silicate melts and glasses at high pressure: Geochimica Et Cosmochimica Acta, v. 68, p. 4189-4200.

Lee, S.K., Kim, H.N., Lee, B.H., Kim, H.I., and Kim, E.J., 2010a, Nature of Chemical and Topological Disorder in Borogermanate Glasses: Insights from B-11 and O-17 Solid-State NMR and Quantum Chemical Calculations: Journal of Physical Chemistry B, v. 114, p. 412-420.

Lee, S.K., Lee, S.B., Park, S.Y., Yi, Y.S., and Ahn, C.W., 2009, Structure of Amorphous Aluminum Oxide: Physical Review Letters, v. 103.

Lee, S.K., Park, S.Y., Yi, Y.S., and Moon, J., 2010b, Structure and Disorder in Amorphous Alumina Thin Films: Insights from High-Resolution Solid-State NMR: Journal of Physical Chemistry C, v. 114, p. 13890-13894.

Lee, S.K., and Stebbins, J.F., 1999, The degree of aluminum avoidance in aluminosilicate glasses: American Mineralogist, v. 84, p. 937-945.

Lee, S.K., and Stebbins, J.F., 2002, Extent of intermixing among framework units in silicate glasses and melts: Geochimica Et Cosmochimica Acta, v. 66, p. 303-309.

Lee, S.K., and Stebbins, J.F., 2009, Effects of the degree of polymerization on the structure of sodium silicate and aluminosilicate glasses and melts: An O-17 NMR study: Geochimica Et Cosmochimica Acta, v. 73, p. 1109-1119.

Levin, I., and Brandon, D., 1998, Metastable alumina polymorphs: Crystal structures and transition sequences: Journal of the American

Ceramic Society, v. 81, p. 1995-2012.

Liebske, C., Behrens, H., Holtz, F., and Lange, R.A., 2003, The influence of pressure and composition on the viscosity of andesitic melts: Geochimica Et Cosmochimica Acta, v. 67, p. 473-485.

Malfait, W.J., Zakaznova-Herzog, V.P., and Halter, W.E., 2008, Quantitative Raman spectroscopy: Speciation of Na-silicate glasses and melts: American Mineralogist, v. 93, p. 1505-1518.

McMillan, P.F., and Hess, A.C., 1990, Ab initio valence force-field calculations for quartz: Physics and Chemistry of Minerals, v. 17, p. 97-107.

McMillan, P.F., and Wolf, G.H., 1995, Vibrational spectroscopy of silicate liquids, Structure, Dynamics and Properties of Silicate Melts, Volume 32: Reviews in Mineralogy, p. 247-315.

McMillan, P.F., Wolf, G.H., and Poe, B.T., 1992, Vibrational spectroscopy of silicate liquids and glasses: Chemical Geology, v. 96, p. 351-366.

Medek, A., Harwood, J.S., and Frydman, L., 1995, Multiple-quantum magic-angle spinning NMR: A new method for the study of quadrupolar nuclei in solids: Journal of the American Chemical Society, v. 117, p. 12779-12787.

Mysen, B.O., 2006, The structural behavior of ferric and ferrous iron in aluminosilicate glass near meta-aluminosilicate joins: Geochimica Et Cosmochimica Acta, v. 70, p. 2337-2353.

Mysen, B.O., and Frantz, J.D., 1993a, Structure and properties of alkali

silicate melts at magmatic temperatures: European Journal of Mineralogy, v. 5, p. 393-407.

Mysen, B.O., and Frantz, J.D., 1993b, Structure of silicate melts at high-temperature in-situ measurements in the system $BaO-SiO_2$: American Mineralogist, v. 78, p. 699-709.

Mysen, B.O., and Virgo, D., 1985, Iron-bearing silicate melts - relations between pressure and redox equilibria: Physics and Chemistry of Minerals, v. 12, p. 191-200.

Mysen, B.O., Virgo, D., Neumann, E.R., and Seifert, F.A., 1985a, Redox equilibria and the structural states of ferric and ferrous iron in melts in the system $CaO-MgO-Al_2O_3-SiO_2-FeO$ - relationships between redox equilibria, melt structure and liquidus phase-equilibria: American Mineralogist, v. 70, p. 317-331.

Mysen, B.O., Virgo, D., Scarfe, C.M., and Cronin, D.J., 1985b, Viscosity and structure of iron-bearing and aluminum-bearing calcium silicate melts at 1-atm: American Mineralogist, v. 70, p. 487-498.

Navrotsky, A., 1995, Energetics of silicate melts, Structure, Dynamics and Properties of Silicate Melts, Volume 32: Reviews in Mineralogy, p. 121-143.

O'Dell, L.A., Savin, S.L.P., Chadwick, A.V., and Smith, M.E., 2007, A Al-27 MAS NMR study of a sol-gel produced alumina: Identification of the NMR parameters of the theta-Al2O3 transition alumina phase: Solid State Nucl. Magn. Reson., v. 31, p. 169-173.

Paglia, G., Buckley, C.E., Rohl, A.L., Hart, R.D., Winter, K., Studer, A.J.,

Hunter, B.A., and Hanna, J.V., 2004, Boehmite derived gamma-alumina system. 1. Structural evolution with temperature, with the identification and structural determination of a new transition phase, gamma '-alumina: Chem. Mater., v. 16, p. 220-236.

Pecharroman, C., Sobrados, I., Iglesias, J.E., Gonzalez-Carreno, T., and Sanz, J., 1999, Thermal evolution of transitional aluminas followed by NMR and IR spectroscopies: Journal of Physical Chemistry B, v. 103, p. 6160-6170.

Pierce, E.M., Reed, L.R., Shaw, W.J., McGrail, B.P., Icenhower, J.P., Windisch, C.F., Cordova, E.A., and Broady, J., 2010, Experimental determination of the effect of the ratio of B/Al on glass dissolution along the nepheline ($NaAlSiO_4$)-malinkoite ($NaBSiO_4$) join: Geochimica Et Cosmochimica Acta, v. 74, p. 2634-2654.

Pollastro, R.M., and Bohor, B.F., 1993, Origin and clay-mineral genesis of the cretaceous-tertiary boundary unit, western interior of North-America: Clays and Clay Minerals, v. 41, p. 7-25.

Rossano, S., Balan, E., Morin, G., Bauer, J.P., Calas, G., and Brouder, C., 1999, Fe-57 Mossbauer spectroscopy of tektites: Physics and Chemistry of Minerals, v. 26, p. 530-538.

Rossano, S., Behrens, H., and Wilke, M., 2008, Advanced analyses of Fe-57 Mossbauer data of alumino-silicate glasses: Physics and Chemistry of Minerals, v. 35, p. 77-93.

Rossano, S., Ramos, A., Delaye, J.M., Creux, S., Filipponi, A., Brouder, C., and Calas, G., 2000, EXAFS and Molecular Dynamics combined

study of CaO-FeO-2$SiO_2$ glass. New insight into site significance in silicate glasses: Europhysics Letters, v. 49, p. 597-602.

Saalfeld, H., and Wedde, M., 1974, Refinement of crystal-structure of gibbsite, $Al(OH)_3$: Zeitschrift Fur Kristallographie, v. 139, p. 129-135.

Sass, B.M., Rosenberg, P.E., and Kittrick, J.A., 1987, The stability of illite smectite during diagenesis - an experimental-study: Geochimica Et Cosmochimica Acta, v. 51, p. 2103-2115.

Sharp, R., Lohr, L., and Miller, J., 2001, Paramagnetic NMR relaxation enhancement: recent advances in theory: Progress in Nuclear Magnetic Resonance Spectroscopy, v. 38, p. 115-158.

Shi, P., and Libourel, G., 1991, The effects of FeO on the system cmas at low-pressure and implications for basalt crystallization processes: Contributions to Mineralogy and Petrology, v. 108, p. 129-145.

Smith, K.A., Kirkpatrick, R.J., Oldfield, E., and Henderson, D.M., 1983, High-resolution Si-29 nuclear magnetic-resonance spectroscopic study of rock-forming silicates: American Mineralogist, v. 68, p. 1206-1215.

Snyder, D., Carmichael, I.S.E., and Wiebe, R.A., 1993, Experimental-study of liquid evolution in an fe-rich, layered mafic intrusion - constraints of Fe-Ti oxide precipitation on the T-$FO_2$ and T-rho paths of tholeiitic magmas: Contributions to Mineralogy and Petrology, v. 113, p. 73-86.

Stebbins, J.F., and Kelsey, K.E., 2009, Anomalous resonances in Si-29 and Al-27 NMR spectra of pyrope ( $Mg,Fe_{(3)}Al_2Si_3O_{12}$) garnets: effects of

paramagnetic cations: Physical Chemistry Chemical Physics, v. 11, p. 6906-6917.

Stebbins, J.F., Panero, W.R., Smyth, J.R., and Frost, D.J., 2009, Forsterite, wadsleyite, and ringwoodite ($Mg_2SiO_4$): Si-29 NMR constraints on structural disorder and effects of paramagnetic impurity ions: American Mineralogist, v. 94, p. 626-629.

Stebbins, J.F., Sen, S., and Farnan, I., 1995, Silicate species exchange, viscosity, and crystallization in a low-silica melt - in-situ high-temperature MAS NMR-spectroscopy: American Mineralogist, v. 80, p. 861-864.

Stebbins, J.F., and Xu, Z., 1997, NMR evidence for excess non-bridging oxygen in an aluminosilicate glass: Nature, v. 390, p. 60-62.

Toplis, M.J., and Carroll, M.R., 1996, Differentiation of ferro-basaltic magmas under conditions open and closed to oxygen: Implications for the Skaergaard intrusion and other natural systems: Journal of Petrology, v. 37, p. 837-858.

Toplis, M.J., and Corgne, A., 2002, An experimental study of element partitioning between magnetite, clinopyroxene and iron-bearing silicate liquids with particular emphasis on vanadium: Contributions to Mineralogy and Petrology, v. 144, p. 22-37.

Violante, A., and Huang, P.M., 1993, Formation mechanism of aluminum hydroxide polymorphs: Clays and Clay Minerals, v. 41, p. 590-597.

Virgo, D., and Mysen, B.O., 1985, The structural state of iron in oxidized vs reduced glasses at 1 atm - a fe-57 mossbauer study: Physics and

Chemistry of Minerals, v. 12, p. 65-76.

Wager, L.R., 1956, A Chemical definition of fractionation stages as a basis for comparison of hawaiian, hebridean, and other basic lavas: Geochimica Et Cosmochimica Acta, v. 9, p. 217-248.

Walter, T.H., and Oldfield, E., 1989, Magic angle spinning O-17 NMR of aluminum-oxides and hydroxides: Journal of Physical Chemistry, v. 93, p. 6744-6751.

Wang, Z.F., Cooney, T.F., and Sharma, S.K., 1993, High-temperature structural investigation of $Na_2O.0.5Fe_2O_3.3SiO_2$ and $Na_2O.FeO.3SiO_2$ melts and glasses: Contributions to Mineralogy and Petrology, v. 115, p. 112-122.

Wang, Z.F., Cooney, T.F., 1995, In-situ structural investigation of iron-containing silicate liquids and glasses: Geochimica Et Cosmochimica Acta, v. 59, p. 1571-1577.

Waychunas, G.A., Brown, G.E., Ponader, C.W., and Jackson, W.E., 1988, Evidence from X-ray absorption for network-forming $Fe^{2+}$ in molten alkali silicates: Nature, v. 332, p. 251-253.

Whitney, G., and Northrop, H.R., 1988, Experimental investigation of the smectite to illite reaction - dual reaction-mechanisms and oxygen-isotope systematics: American Mineralogist, v. 73, p. 77-90.

Wilke, M., Farges, F., Partzsch, G.M., Schmidt, C., and Behrens, H., 2007, Speciation of Fe in silicate glasses and melts by in-situ XANES spectroscopy: American Mineralogist, v. 92, p. 44-56.

Wilke, M., Farges, F., Petit, P.E., Brown, G.E., and Martin, F., 2001, Oxidation state and coordination of Fe in minerals: An Fe K-XANES spectroscopic study: American Mineralogist, v. 86, p. 714-730.

Xue, X.Y., Stebbins, J.F., and Kanzaki, M., 1994, Correlations between O-17 NMR parameters and local-structure around oxygen in high-pressure silicates - implications for the structure of silicate melts at high-pressure: American Mineralogist, v. 79, p. 31-42.

Zhou, R.S., and Snyder, R.L., 1991, Structures and transformation mechanisms of the eta, gamma and theta transition aluminas: Acta Crystallographica Section B-Structural Science, v. 47, p. 617-630.

Zigan, F., Joswig, W., and Burger, N., 1978, hydrogen positions in bayerite, $Al(OH)_3$: zeitschrift fur kristallographie, v. 148, p. 255-273.

## Figures

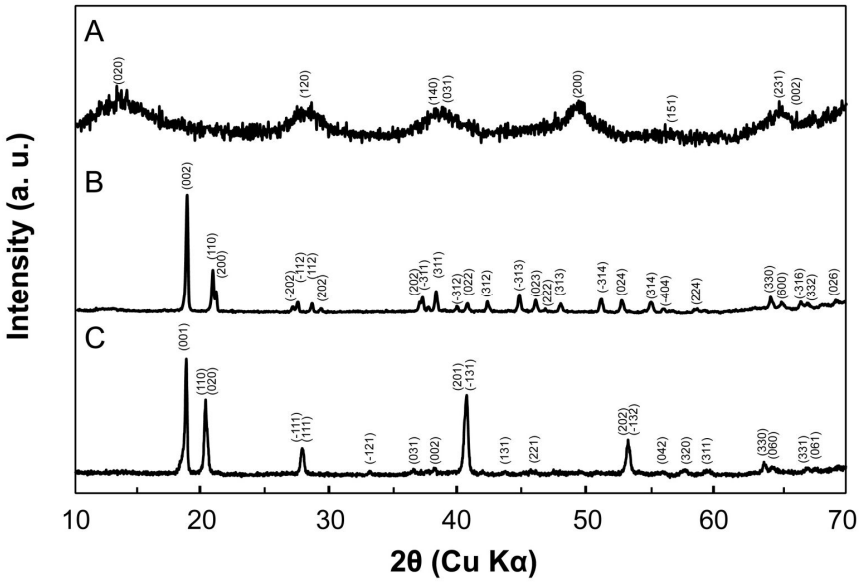


**Figure 1.** X-ray diffraction patterns for aluminum (oxy)hydroxide polymorphs. (A) boehmite, (B) gibbsite, and (C) bayerite

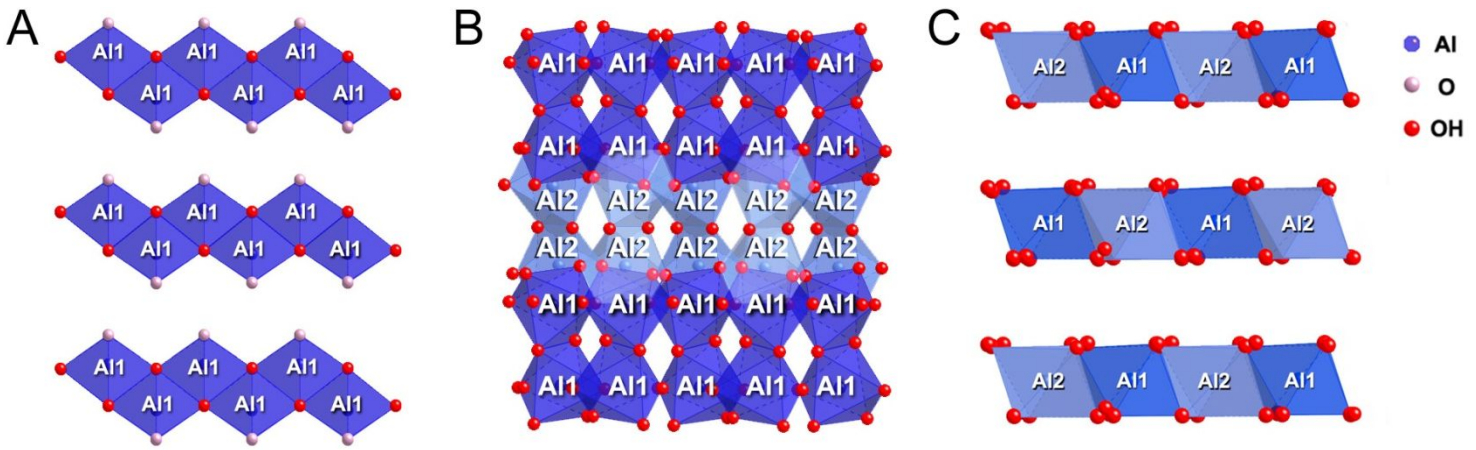


**Figure 2.** Crystal structures of aluminum (oxy)hydroxide polymorphs. (A) boehmite, (B) gibbsite, and (c) bayerite. $AlO_6$ polyhedra are shown in blue and sky blue, O atoms in pink and O atoms with hydrogen bond in red.

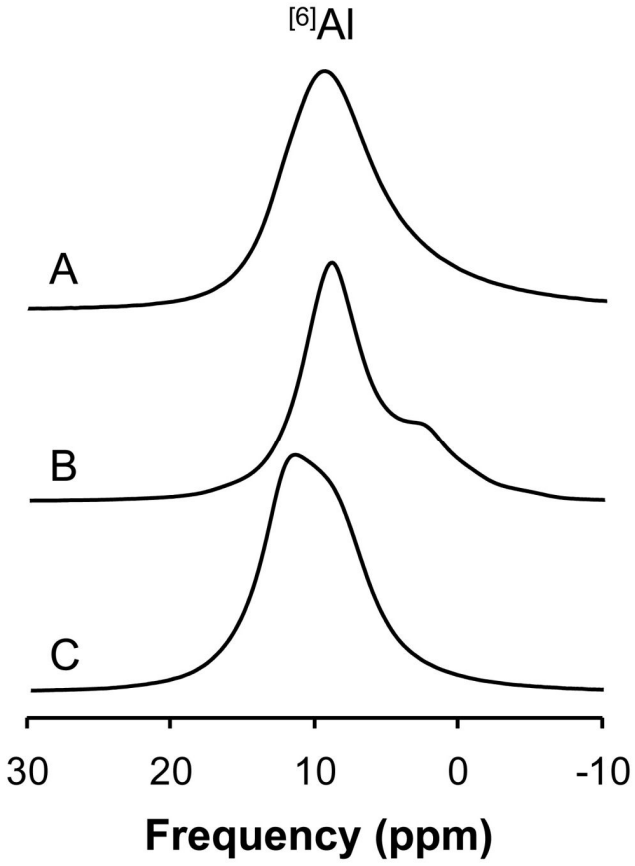


**Figure 3.** $^{27}$Al MAS NMR spectra for aluminum (oxy)hydroxide polymorphs at 11.7 T. (A) boehmite, (B) gibbsite, and (C) bayerite.

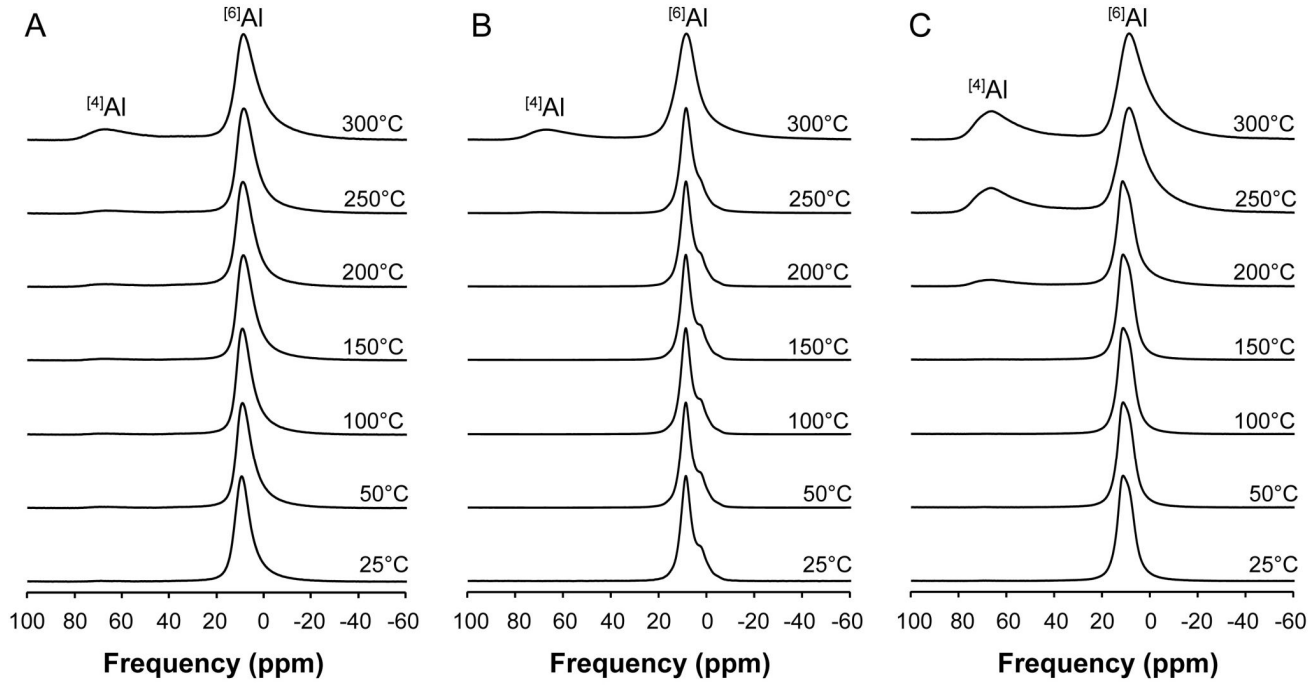


**Figure 3.** $^{27}$Al MAS NMR spectra for aluminum (oxy)hydroxide polymorphs at 11.7 T. (A) boehmite, (B) gibbsite, and (C) bayerite.

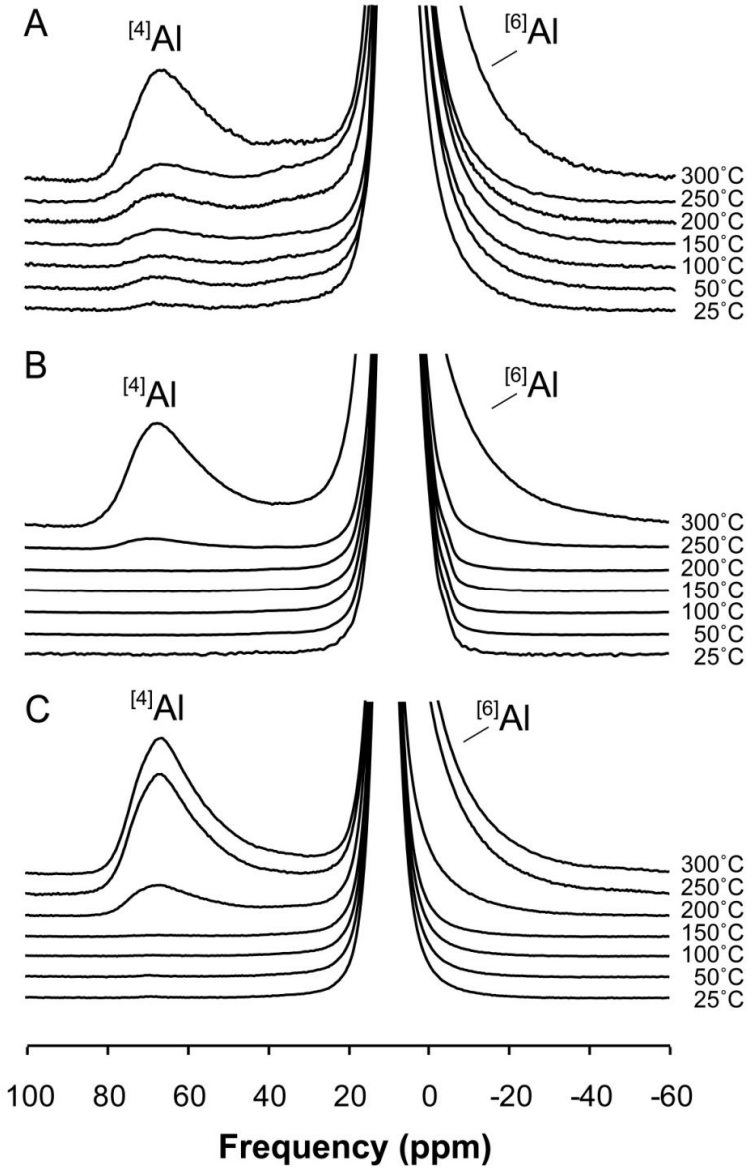


**Figure 5.** $^{27}$Al MAS NMR spectra for (A) boehmite, (B) gibbsite, and (C) gibbsite with varying annealing temperature at 11.7 T. Vertical scales enlarged by 5× (A and B) and 3× (C) from Figure 4.

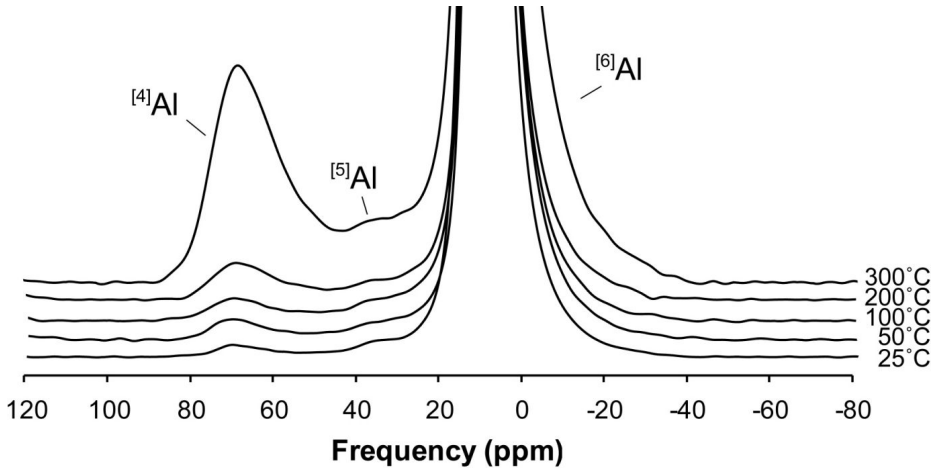


**Figure 6.** $^{27}$Al MAS NMR spectra for boehmite with varying annealing temperature at 14.1 T

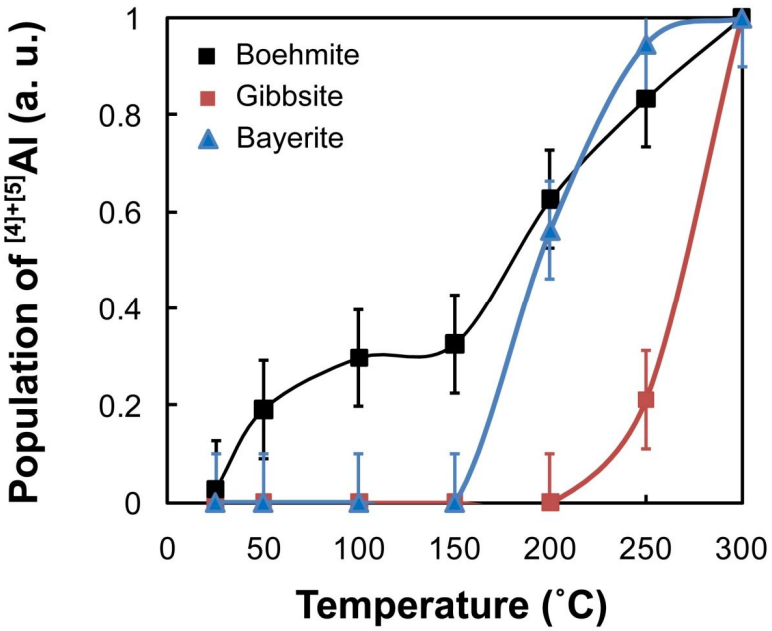


**Figure 7.** The variation of [4,5]Al population for series of aluminum (oxy)hydroxide polymorphs below 300℃. Each value is normalized by the [4,5]Al fraction at 300°C.

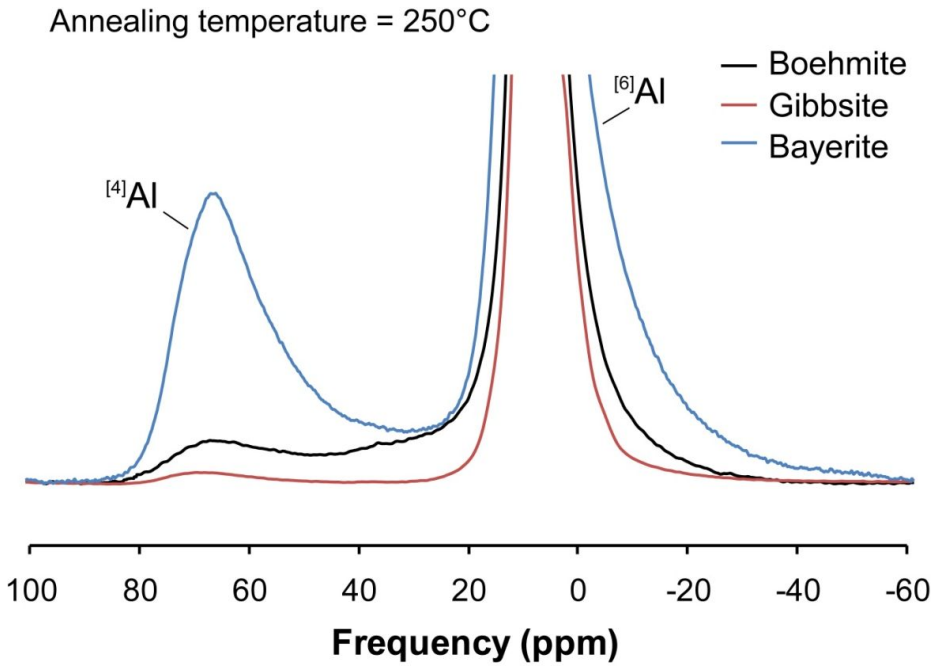


**Figure 8.** $^{27}$Al MAS NMR spectra for annealed aluminum (oxy)hydroxide polymorphs at 250°C (11.7 T)

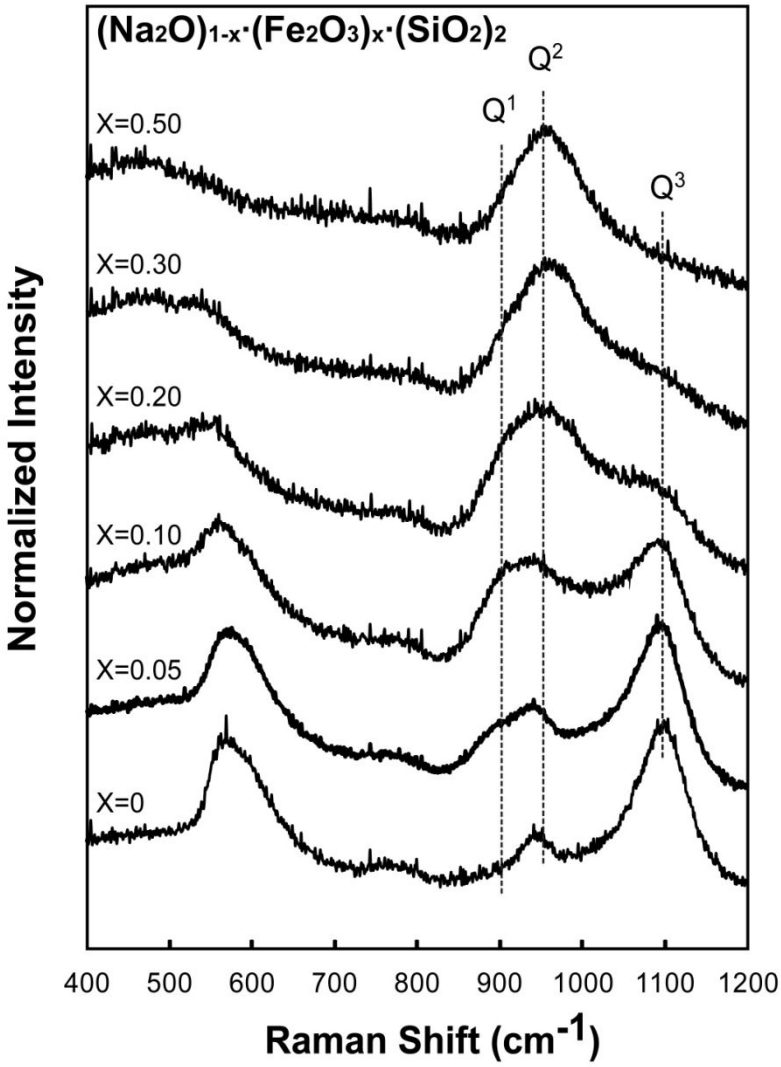


**Figure 9.** Normalized Raman spectra for iron-bearing sodium silicate glasses at 9.4 T with varying $X_{Fe_2O_3}$ [=$Fe_2O_3$/($Fe_2O_3$+$Na_2O$)], as labeled.

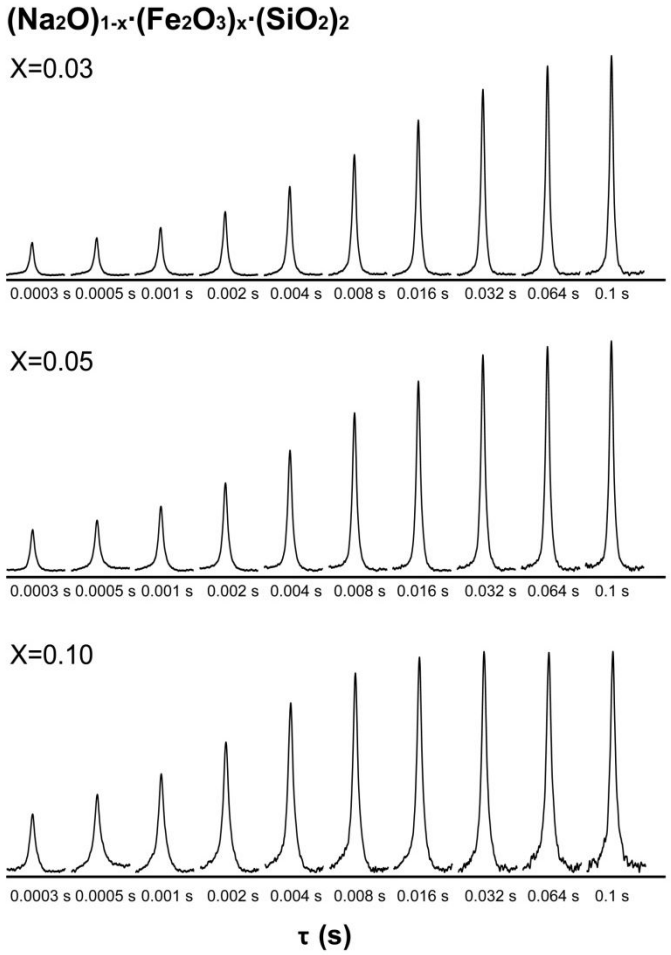


**Figure 10.** $^{29}$Si MAS NMR spectra for iron-bearing sodium silicate glasses at τ from 0.0003 to 0.1 s with varying $X_{Fe_2O_3}$ [=$Fe_2O_3$/($Fe_2O_3$+$Na_2O$)], as labeled.

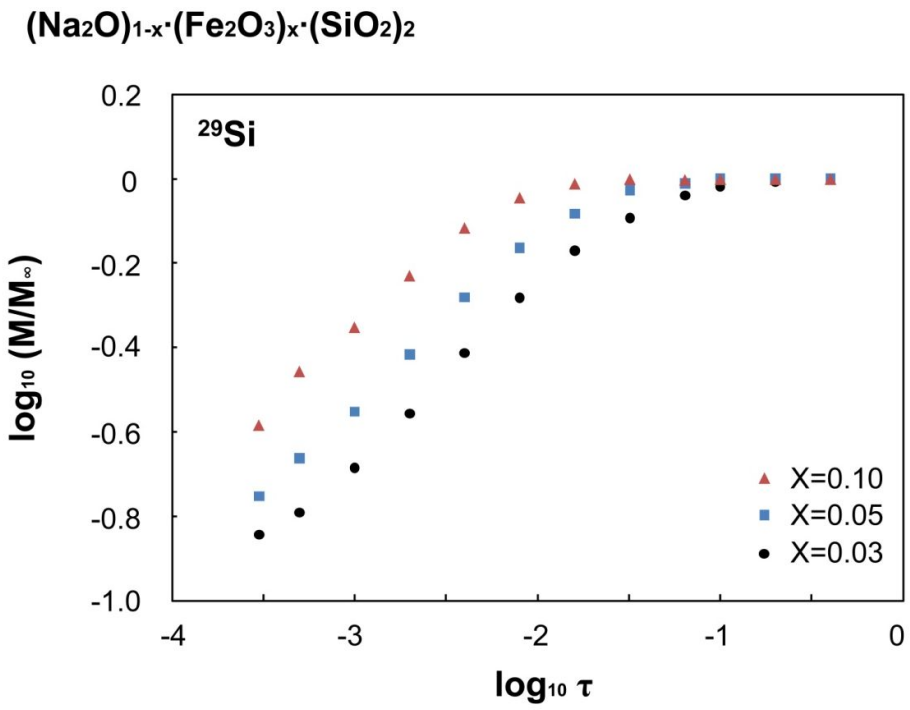


**Figure 11.** $\log_{10}$-$\log_{10}$ plot of $^{29}Si$ $T_1$ relaxation (saturation-recovery) data for iron-bearing sodium silicate glasses at 9.4 T with varying $X_{Fe_2O_3}$ [=$Fe_2O_3$/($Fe_2O_3$+$Na_2O$)], as labeled.

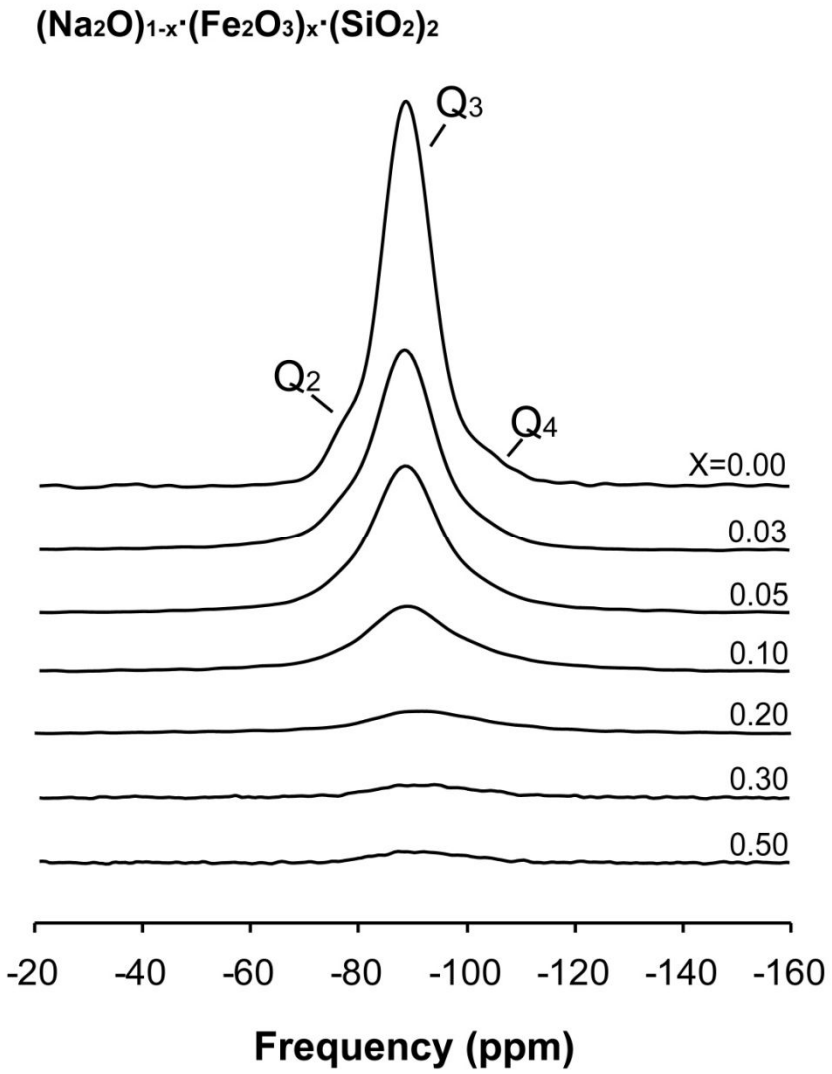


**Figure 12.** $^{29}$Si MAS NMR for iron-bearing sodium silicate glasses at 9.4 T with varying $X_{Fe_2O_3}$ [=$Fe_2O_3$/($Fe_2O_3$+$Na_2O$)], as labeled. Vertical scale is arbitral unit (not normalized) due to comparison of signal intensity with increasing $X_{Fe_2O_3}$.

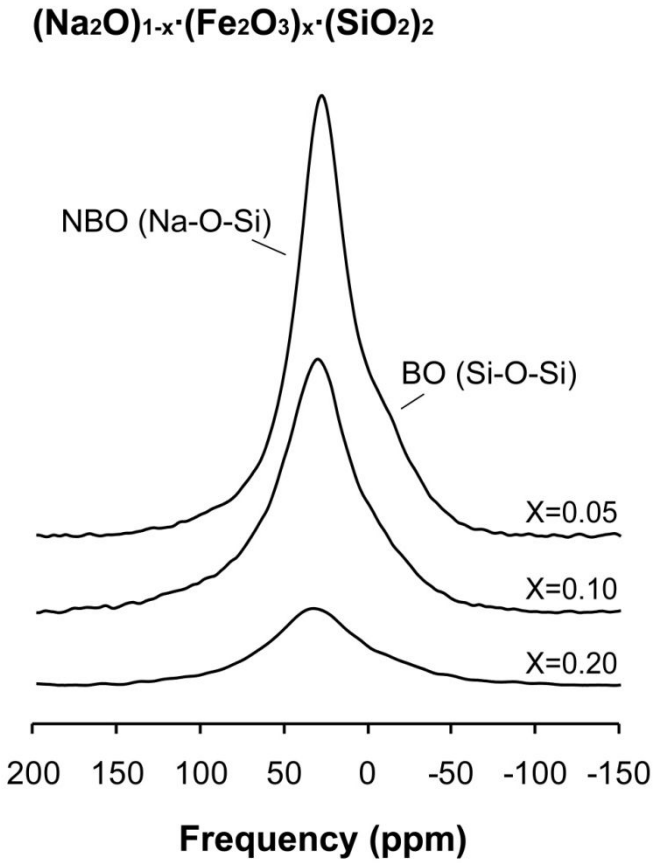


**Figure 13.** $^{17}O$ MAS NMR spectra for iron-bearing sodium silicate glasses at 9.4 T with varying $X_{Fe_2O_3}$ [=$Fe_2O_3$/($Fe_2O_3$+$Na_2O$)], as labeled. Vertical scale is arbitral unit (not normalized) due to comparison of signal intensity with increasing $X_{Fe_2O_3}$

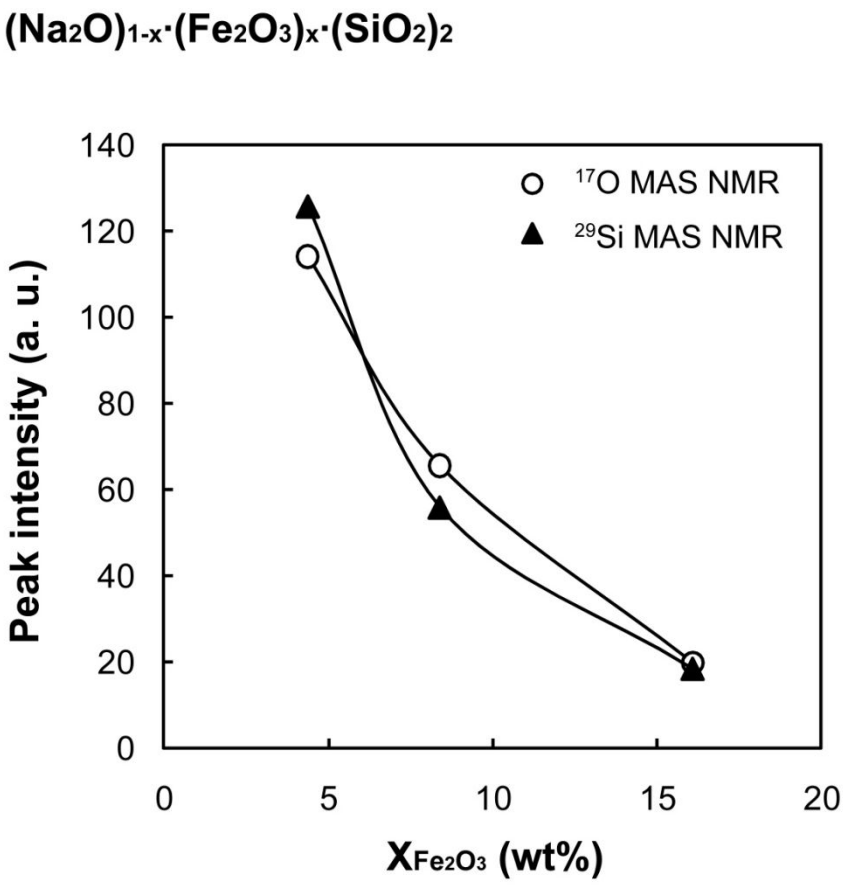


**Figure 14.** Variation of maximum peak intensity for $^{29}Si$ (closed triangle) and $^{17}O$ (open circle) MAS NMR spectra with varying $X_{Fe_2O_3}$.

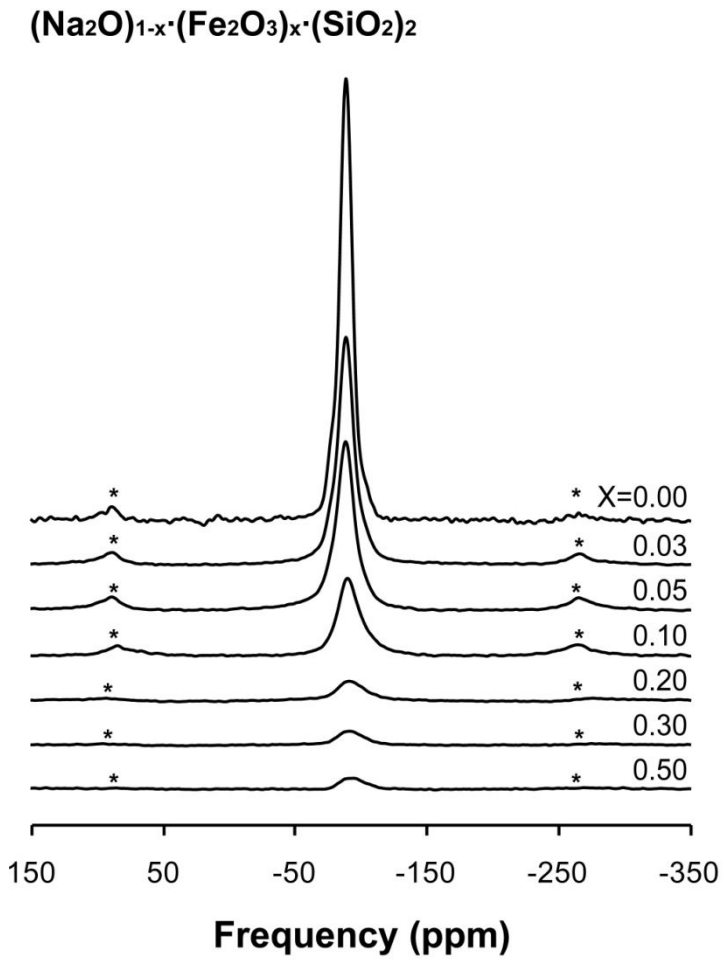


**Figure 15.** $^{29}$Si MAS NMR spectra for iron-bearing sodium silicate glasses at 9.4 T with varying $X_{Fe_2O_3}$ [=$Fe_2O_3$/($Fe_2O_3$+$Na_2O$)], as labeled. The spinning side band is also presented in this Figure. Vertical scale is arbitral unit (not normalized) due to comparison of signal intensity with increasing $X_{Fe_2O_3}$.

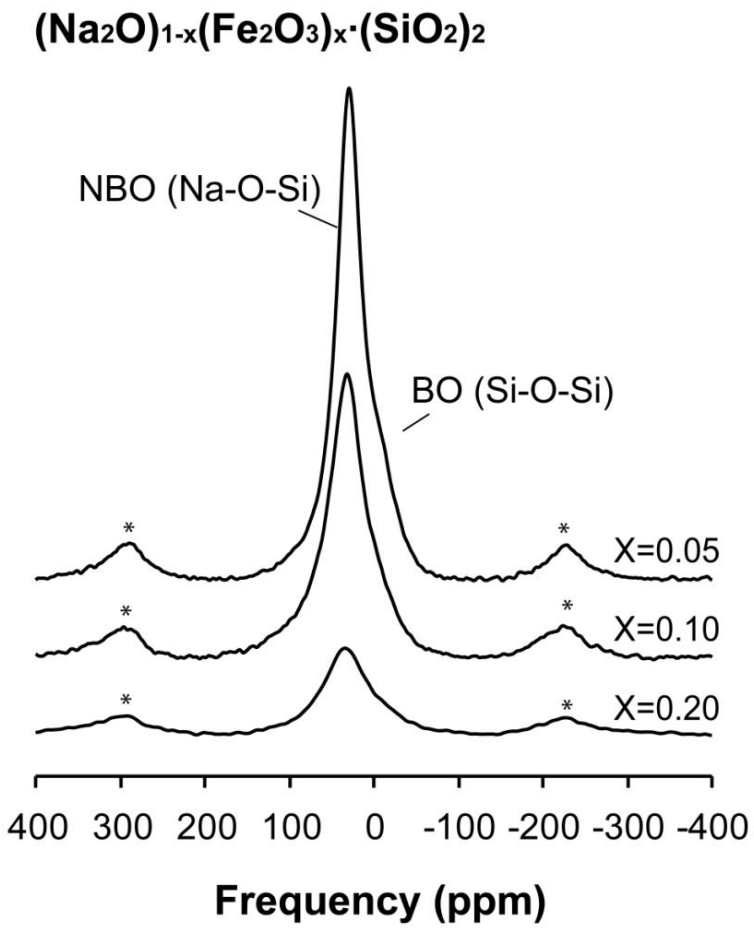


**Figure 16.** $^{17}O$ MAS NMR spectra for iron-bearing sodium silicate glasses at 9.4 T with varying $X_{Fe_2O_3}$ [=$Fe_2O_3$/($Fe_2O_3$+$Na_2O$)], as labeled. The spinning side band is also presented in this Figure. Vertical scale is arbitral unit (not normalized) due to comparison of signal intensity with increasing $X_{Fe_2O_3}$.

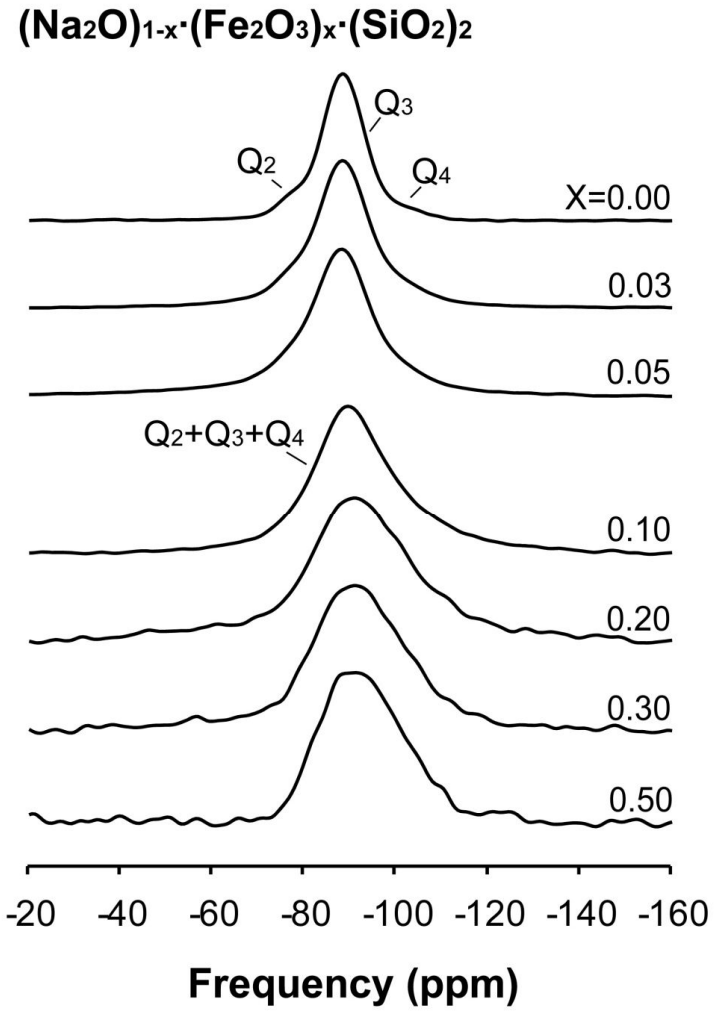


**Figure 17.** Normalized $^{29}Si$ MAS NMR spectra for iron-bearing sodium silicate glasses at 9.4 T with varying $X_{Fe_2O_3}$ [=$Fe_2O_3$/($Fe_2O_3$+$Na_2O$)], as labeled.

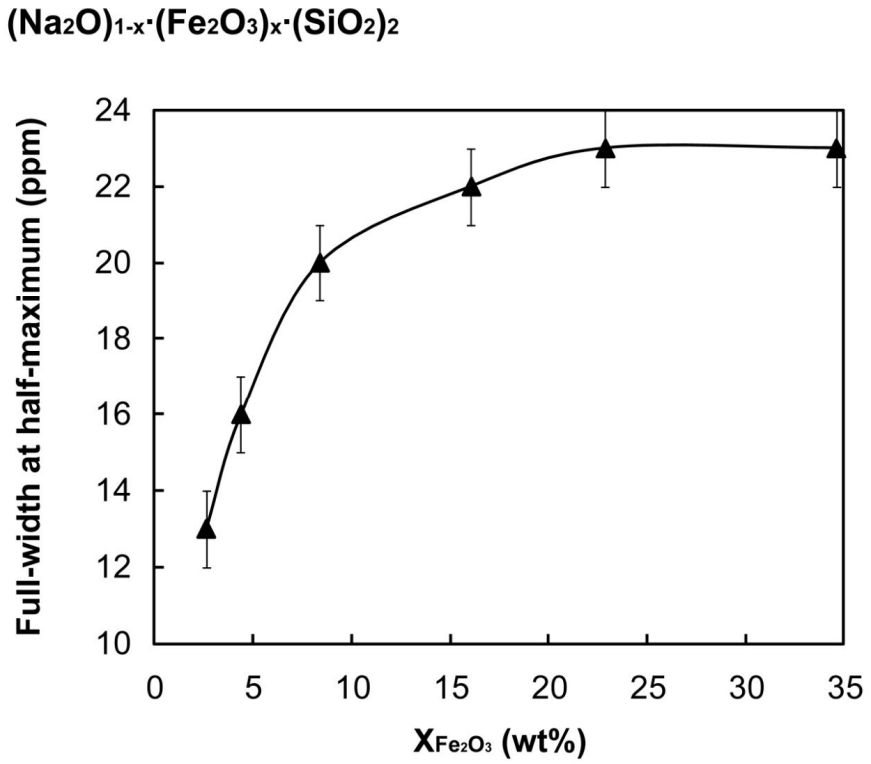


**Figure 18.** Variation of full width at half maximum (FWHM) of $^{29}Si$ MAS NMR spectra for iron-bearing sodium silicate glasses at 9.4 T with varying $X_{Fe_2O_3}$ [=$Fe_2O_3$/($Fe_2O_3$+$Na_2O$)], as labeled.

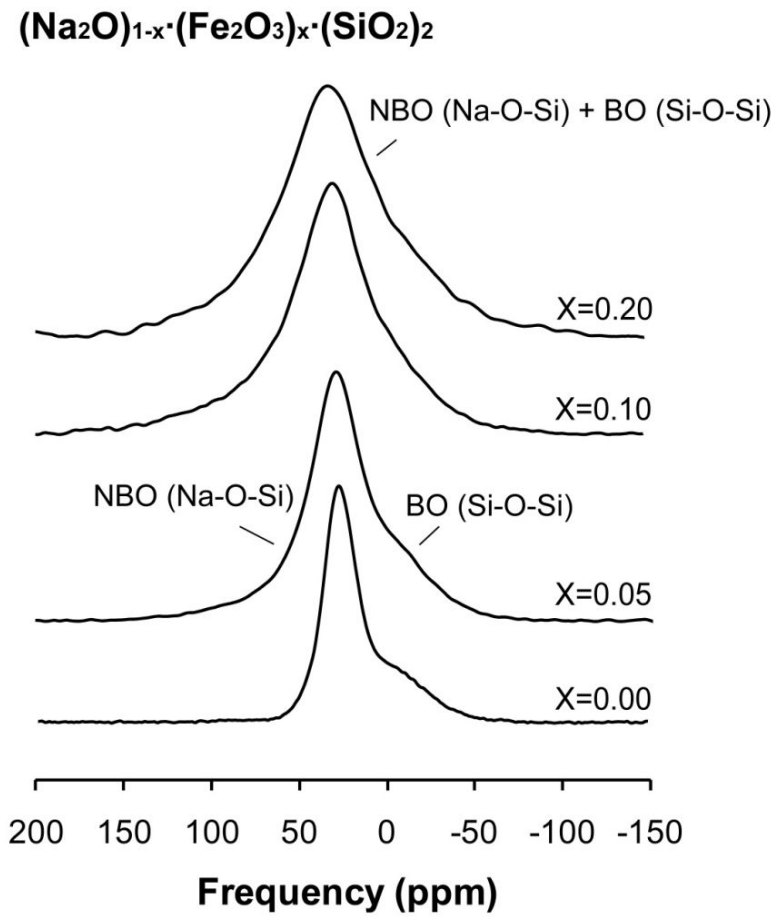


**Figure 19.** Normalized $^{17}O$ MAS NMR spectra for iron-bearing sodium silicate glasses at 9.4 T with varying $X_{Fe_2O_3}$ [=$Fe_2O_3$/($Fe_2O_3$+$Na_2O$)], as labeled.

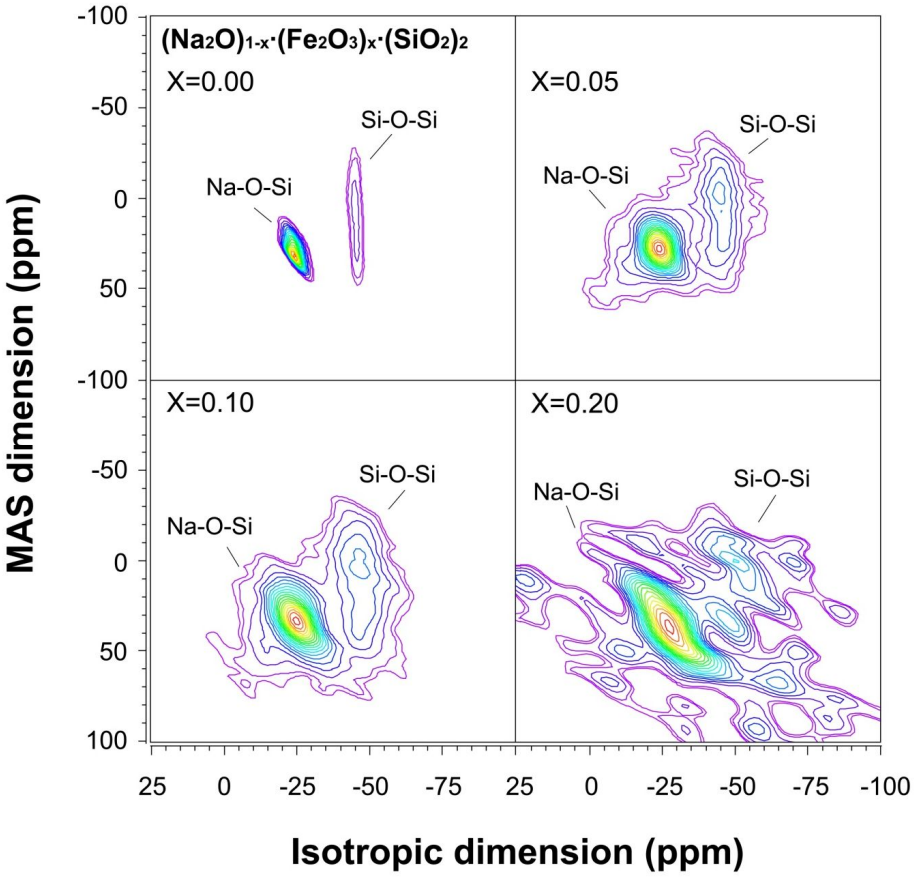


**Figure 20.** $^{17}O$ 3QMAS NMR for iron-bearing sodium silicate glasses at 9.4 T with varying $X_{Fe_2O_3}$ [=$Fe_2O_3$/($Fe_2O_3$+$Na_2O$)], as labeled. Contour lines are drawn from 8% to 98% of relative intensity with a 5% increment and an added line at 6%.

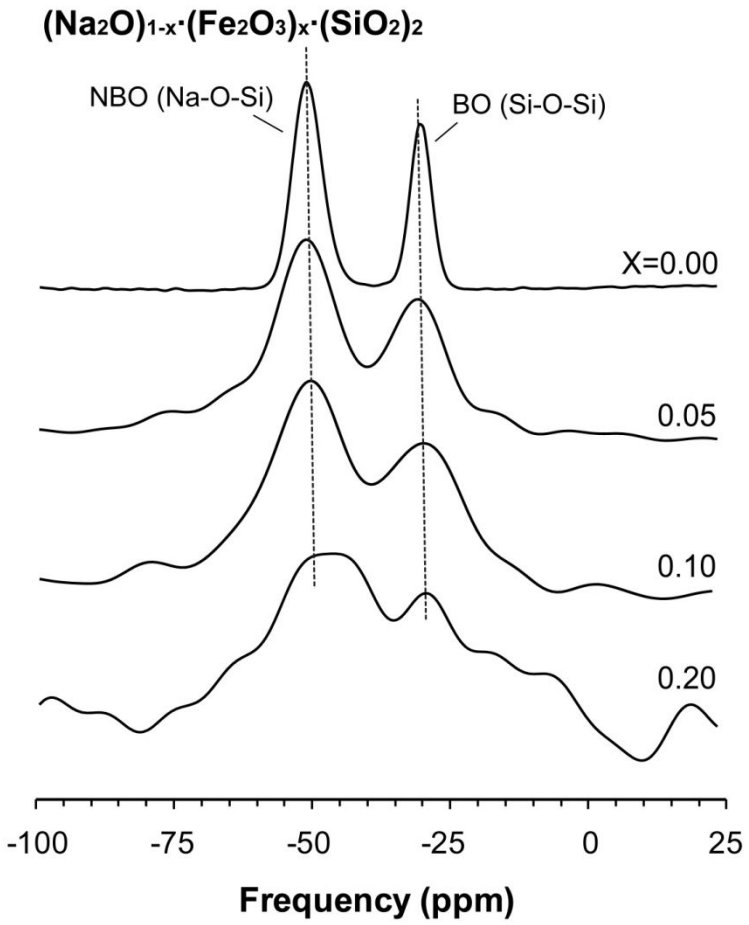


**Figure 21.** Total isotropic projection of $^{17}O$ 3QMAS NMR for iron-bearing sodium silicate glasses at 9.4 T with varying $X_{Fe_2O_3}$ [=$Fe_2O_3$/($Fe_2O_3$+$Na_2O$)], as labeled.

## Tables

| Crystal | Composition | Lattice Parameter | | | | | | |
|---|---|---|---|---|---|---|---|---|
| | | Space Group(number) | a (Å) | b (Å) | c (Å) | α (°) | β (°) | γ (°) |
| Boehmite[1] | γ-AlOOH | Cmcm(36) | 2.848 | 12.227 | 3.7 | 90 | 90 | 90 |
| Gibbsite[2] | γ-$Al(OH)_3$ | P2(1)/n(14) | 8.684 | 5.078 | 9.736 | 90 | 94.54 | 90 |
| Bayerite[3] | α-$Al(OH)_3$ | P2(1)/n(14) | 5.062 | 8.671 | 4.713 | 90 | 90.27 | 90 |

[1] Tertian and Papee, 1958

[2] Saalfeld and Wedde, 1974

[3] Rothbauer et al., 1967

**Table 1.** Space groups and lattice parameters of aluminum (oxy)hydroxide polymorphs.

| $X_{Fe_2O_3}$ | Mole% (nominal) | | | Weight% (nominal) | | |
|---|---|---|---|---|---|---|
| | $Na_2O$ | $Fe_2O_3$ | $SiO_2$ | $Na_2O$ | $Fe_2O_3$ | $SiO_2$ |
| 0 | 33.33 | 0 | 66.67 | 33.66 | 0 | 66.34 |
| 0.03 | 32.33 | 1.00 | 66.67 | 31.98 | 2.60 | 65.41 |
| 0.05 | 31.67 | 1.67 | 66.67 | 30.63 | 4.39 | 64.98 |
| 0.10 | 30.00 | 3.33 | 66.67 | 28.94 | 8.38 | 62.68 |
| 0.20 | 26.67 | 6.67 | 66.67 | 23.76 | 16.07 | 60.16 |
| 0.30 | 23.33 | 10.00 | 66.67 | 19.70 | 22.88 | 57.42 |
| 0.50 | 16.67 | 16.67 | 66.67 | 13.22 | 34.60 | 52.18 |

**Table 2.** Composition of $Na_2O$-$Fe_2O_3$-$SiO_2$ silicate glasses with varying $Fe_2O_3$ content. $X_{Fe_2O_3}$ is the mole fraction of $Fe_2O_3$

# Appendix

**Appendix 1** Nature of chemical and topological disorder in borogermanate glasses: Insights from B-11 and O-17 solid-state NMR and quantum chemical calculations

(Lee, S. K., Kim, H. N., Lee, B. H., Kim, H. I., Kim, E. J., J. Phys. Chem. B., 2010)

Knowledge of the extent of chemical and topological disorder in topological disordered oxide glasses and melts is essential for understanding the atomistic origins of their macroscopic properties. Here, we report the high-resolution B-11 and O-17 triple quantum magic angle spinning (3QMAS) NMR spectra for binary borogermanate glasses. The NMR results, together with quantum chemical calculations of cluster energy difference, allow us to estimate the extent of chemical disorder and topology variation with composition. The B-11 NMR result shows that the boroxol ring fraction decreases nonlinearly with increasing mole fraction of Ge and is smaller than that in binary borosilicate glasses, suggesting that the Ge/Si content influences the topological changes. Whereas oxygen clusters are not well resolved in O-17 NMR spectra, the Ge-O-Ge fraction apparently increases with increasing GeO2 content. The estimated degree of framework disorder (Q) in borogermanate glasses is approximately 0.4, according to quantum chemical calculations based on density functional theory. This is halfway between chemical order (Q=1) and a random distribution (Q=0). In contrast, Q is approximately -0.6 for borosilicate glasses, indicating a moderate tendency toward complete phase separation

(Q=-1). This result confirms that the degree of framework disorder shows a strong dependence on the type of framework cations (Si or Ge). The predicted configurational enthalpy of borogermanate glasses, explicitly considering both chemical and topological disorder, shows a negative deviation as predicted from the positive Q value. The results demonstrate that the macroscopic properties of topologically disordered noncrystalline solids can be established from the detailed quantification of topological and chemical disorder.

## Appendix 2 C. V.

EDUCATION

2009. 8 B. S. Seoul National University, Korea. Earth Science Education

B. S. Seoul National University, Korea. School of Earth Environmental Science

RESEARCH EXPERIENCE

2007 – 2008 Research assistant, Seoul National University, Meteorite Research Lab

2010. 9 – 12 Teaching assistant, Seoul National University

HONORS & AWARDS

2011. 5 우수포스터상 수상, 한국광물학회

2011. 3 자연대 발전기금 장학금 수여

2010. 9 자연대 발전기금 장학금 수여

2009. 8 2009년 후반기 환경안전교육 최우수상 표창, 서울대학교 환경안전원

2009. 5 제 1 회 한국광물학회 학생 사진전 장려상 수상, 한국광물학회

PUBLICATIONS

[1] Lee, S.K., Kim, H.N., Lee, B.H., Kim, H.I., Kim, E.J., Nature of chemical and topological disorder in borogermanate glasses: Insights from B-11 and O-17 solid-state NMR and quantum chemical calculations, Journal of

Physical Chemistry B, 114 412 (2010)

CONFERENCES

2011. 5 고상 핵자기공명 분광분석을 이용한 수산화알루미늄의 상전이 기작에 대한 원자단위의 규명 (Oral), 2011년 한국광물학회 학술발표회

2011. 5 철의 함량에 따른 Fe-규산염 비정질의 원자구조 및 무질서도 변화에 대한 원자단위의 고찰: 고분해능 고상 핵자기 공명 분광분석을 이용한 연구 (Poster), 2011년 한국광물학회 학술발표회

2010. 10 300°C 이하 온도 영역에서 준안정상 알루미늄 화합물 상전이 기작에 대한 원자단위의 규명: 고분해능 고상 핵자기공명 분광분석 연구 (Oral), 2010년 추계지질과학연합 학술발표회

2009. 5 미분화운석 내 콘드률의 이심률 및 배열경향성 분석 (Poster), 2009년, 한국암석학회 학술발표회

## 국문 요약

물질이 갖는 열역학적 성질이나 이동 성질과 같은 거시적인 성질은 물질을 구성하는 원자 단위의 구조적인 배열, 화학적인 분배 등의 원자 단위의 정보를 통해 이해할 수 있다. 이 때 물질을 구성하는 원자의 구조는 온도, 압력, 조성과 같은 다양한 변수를 통해 결정되므로 이와 같은 미시적인 관점의 지구물질 연구는 궁극적으로 주어진 환경에서의 거시적인 물성뿐만 아니라 전지구적인 물질의 거동을 설명할 수 있는 중요한 단서가 된다. 그러므로 물질의 원자 단위의 정보를 정량화하는 것은 지구물질과학 및 일반 물리, 화학 분야에서도 중요한 연구 과제로 여겨지고 있다. 이러한 중요성에도 불구하고 300℃ 이하의 저온에서 일어나는 온도에 따른 원자 구조의 변화와 철이 포함된 비정질 규산염 용융체의 원자단위의 정보, 즉 원자구조나 무질서도를 알아내는 일은 실제 실험적인 방법을 통해 밝혀내는 것에 한계가 있기 때문에 과학 전반적인 분야에 걸쳐 아직 풀리지 못한 난제로 남아있다.

300℃ 이하의 온도 영역에서 수산화알루미늄은 온도가 상승함에 따라 준안정상으로의 상전이가 일어난다. 이러한 물질의 상전이 과정을 이해하는 것은 지표면에서 일어나는 풍화, 변질, 그리고 속성작용과 같은 복잡한 지질학적 현상을 이해하는데 도움을 준다. 특히 수산화알루미늄의 경우 상대적으로 간단한 조성을 가지고 있는 것과 동시에 다양한 동질이상을 가지고 있기 때문에 온도와 더불어 상전이 과정에 영향을 미치는 다른 요소들에 의한 영향을 관찰하는데 효과적으로 사용될 수 있다. 고분해능의 고상 핵자기공명 분광분석

(NMR)은 다양한 동질이상을 갖는 수산화알루미늄의 상전이 과정 중에 온도에 따라 미묘하게 변화하는 원자환경까지 정밀하게 관찰할 수 있으며 원자단위의 연결 상태를 보다 정확하고 정량적으로 규명할 수 있게 한다. 따라서 본 연구에서는 고상 핵자기공명 분광분석을 이용하여 300°C 이하 환경에서 온도에 따른 수산화알루미늄의 상전이 과정 중 변화하는 알루미늄 주변의 원자환경을 관찰함으로써 각 물질의 상전이 기작과 관련하는 원자구조 및 무질서도를 규명하고자 하였다.

상온에서의 서로 다른 세 개의 초기 상태 (보헤마이트, 깁싸이트, 베이어라이트)를 갖는 수산화알루미늄의 $^{27}$Al MAS NMR 스펙트럼을 살펴보면 모두 $^{[6]}$Al의 배위수를 갖는 알루미늄만으로 이루어져 있음을 알 수 있다. 이 때 각각의 상태에 따라 약간씩 다른 스펙트럼 모양을 보이고 있는데 이는 각 동질이상이 서로 다른 알루미늄 환경으로 이루어져 있다는 것을 지시한다. 이 세 개의 초기 상태에서 모두 온도가 상승함에 따라 4와 5의 배위수를 갖는 알루미늄 ($^{[4,5]}$Al) 의 비율이 증가하고 $^{[6]}$Al의 피크의 폭이 넓어지고 있음을 알 수 있다. 이와 같은 저온 영역에서의 알루미늄 환경의 변화는 상대적으로 미묘한 변화이므로 기존 연구에서 명확히 보고되지 못하였지만 본 연구의 고해상도의 실험을 통해 저온영역에서 $^{[4,5]}$Al의 존재 여부뿐만 아니라 초기 수산화알루미늄의 형태에 따라 $^{[4,5]}$Al의 비율 변화양상이 확연하게 다르게 나타난다는 것을 확인하였다. 보헤마이트에서 $\gamma$-$Al_2O_3$로 전이되는 경우 $^{[4,5]}$Al이 점진적으로 증가하는 양상을 보이지만 깁싸이트에서 $\gamma$-$Al_2O_3$로, 베이어라이트에서 $\eta$-$Al_2O_3$로 전이되는 경우 특정 온도를 중심으로 급격하게 증가하고 있는 $^{[4,5]}$Al이 관찰된다. 또한

다른 시료에서는 나타나지 않는 [5]Al이 보헤마이트 계열에서 명확하게 나타나고 있는데 이것은 다른 수산화알루미늄에 비해 상대적으로 큰 무질서도 (topological disorder)를 반영한 것으로 이와 같은 보헤마이트 계열의 큰 무질서도는 점진적으로 증가하는 상전이 경향에 영향을 미친 것으로 유추된다. 이렇게 얻어진 결과를 통해 수산화알루미늄의 온도에 따른 상전이 과정에는 온도 뿐만 아니라 초기 물질의 상태 역시 중요한 변수로 작용하고 있음을 알 수 있으며 이는 상대적으로 복잡하고 불균질한 지표면의 물질에서 나타나는 속성작용 중의 상전이 과정을 이해하는데 도움을 줄 수 있을 것으로 기대된다.

철이 포함된 규산염 용융체는 지구의 화성활동의 주체가 되는 마그마를 구성하고 있는 주요 물질이며 맨틀-핵 경계에 존재한다고 알려진 초저속도층을 설명할 수 있는 중요한 지질학적 의미를 갖는 물질이다. 특히 철은 지구 전체를 구성하는 전이 원소 중 가장 높은 비율을 차지하고 있으며 아주 적은 양의 존재만으로도 구성 물질의 광학적, 물리적인 성질들에 큰 영향을 미치기 때문에 철을 포함한 규산염 용융체를 연구하는 것은 지구 내부 물질의 물성 변화를 이해하는 것에 대한 실마리를 제공한다. 이와 같은 중요성에도 불구하고 철이 포함된 규산염 비정질의 원자구조 및 무질서도에 대한 연구는 쉽게 이루어지지 못하고 있는데 이는 철의 두 가지 산화상태에 따른 원자구조 내의 철의 역할이 완전히 알려져 있지 않을 뿐만 아니라 이와 같은 원자구조를 직접적으로 연구할 수 있는 실험 방법이 부재했기 때문이다. 하지만 NMR의 경우 특정 원자 주변의 환경을 직접적으로 관찰하여 원자 간의 중합도 및 연결도에 대한 정보를 제시하므로 규산염 비정질의

원자구조를 규명하는데 강력한 방법론으로 사용되고 있다. 그렇지만 철이 포함된 규산염 용융체 내에 존재하는 상자성 원소 (예. 철)로 인한 NMR 신호와 분해능의 감소 및 각 피크가 넓어지는 현상으로 인해 그동안 철이 포함된 물질에 있어 NMR 방법이 이용되는 것은 거의 불가능해 보였다. 하지만 본 연구에서는 철이 포함된 알칼리 규산염 비정질의 $^{29}$Si와 $^{17}$O MAS NMR과 $^{17}$O 3QMAS NMR 스펙트럼을 제공하며 상자성 원소가 포함된 규산염 비정질 물질에 대한 원자구조의 정보를 최초로 제시하고자 한다.

먼저, 철이 포함된 알칼리 규산염 비정질의 $^{29}$Si의 $T_1$ 이완시간의 경우 상자성 원소가 가지고 있는 홀전자 (unpaired electron)와 핵 스핀 (nuclear spin)이 갖는 상호작용이 커지기 때문에 철의 함량이 증가함에 따라 $T_1$ 이완시간이 짧아지는 것을 확인할 수 있다. 이 결과는 철이 자기환경 하에서 규산염 비정질의 이완을 빠르게 한다는 원자단위의 정보 외에 NMR 실험 방법상에 도움을 주기도 한다. 상자성 원소로 인해 NMR 방법에 어려움이 뒤따르지만 짧은 $T_1$ 이완시간을 갖는 물질의 경우 빠른 시간 내에 동일 실험을 많이 반복할 수 있게 하므로 신호 대 잡음의 비율을 크게 향상시킬 수 있는 효과를 준다. 이와 같은 짧은 $T_1$ 이완시간을 이용하여 얻어진 철이 포함된 알칼리 규산염 비정질의 $^{29}$Si와 $^{17}$O MAS NMR 결과를 살펴보자. 먼저 $^{29}$Si MAS NMR의 스펙트럼을 보면 비교적 적은 비율의 철이 함유된 물질의 경우 $Q^2$, $Q^3$ 그리고 $Q^4$가 부분적으로 분해되지만 철의 함량에 따라 피크의 폭이 증가하여 철의 함량이 높은 물질의 경우 구분이 거의 불가능한 모습을 볼 수 있다. 하지만 피크의 폭이 증가하는 양상을 살펴보면 특정 방향,

특히 $Q^4$ 피크의 방향으로 넓어지고 있음을 알 수 있다. $^{17}O$ MAS NMR 결과도 역시 높은 철의 함량을 갖는 물질에서는 NBO와 BO의 구분이 거의 불가능하지만 $^{29}Si$의 결과와 마찬가지로 피크 폭의 증가 양상이 특정 방향으로 이루어지고 있다. 이와 같은 철의 함량에 따른 피크 폭의 넓어짐 현상이 특정방향으로 강화되고 있다는 결과를 통해 철 주변의 $Q^n$과 NBO, BO가 불균질하게 분포하고 있음을 유추할 수 있다. 철이 포함된 알칼리 규산염 비정질의 2차원 $^{17}O$ 3QMAS NMR 결과는 철의 함량에 따라 그 피크 폭은 MAS 결과와 마찬가지로 넓어지고 있음에도 불구하고 NBO와 BO가 잘 분해되고 있음을 알 수 있다. 이 결과를 통하여 철이 포함된 규산염 비정질의 철의 함량에 따른 산소 주변의 원자 환경, 중합도 및 연결도와 무질서도에 대한 정보를 정량화하여 얻을 수 있게 된다. 이와 같은 결과를 통해 상자성 원소가 포함된 물질의 원자정보를 얻는 것에 그 동안 한계가 있다고 알려져 왔던 NMR이 고유의 장점을 유지하여 철이 포함된 규산염 비정질의 원자단위의 직접적인 정보를 주는 데 효과적으로 이용될 수 있다는 사실과 함께, 특히 $^{17}O$ 3QMAS NMR을 이용하여 고분해능의 데이터를 얻을 수 있음을 제시한다.